Kinetic Solar Envelope

Performance Assessment of a Shape Memory Alloy-Based Autoreactive Façade System for Urban Heat Island Mitigation in Athens, Greece

Koukelli, Christina ; Prieto Hoces, A.I.; Aut, S.

Important note
To cite this publication, please use the final published version (if applicable).
Please check the document version above.

Article

Kinetic Solar Envelope: Performance Assessment of a Shape Memory Alloy-Based Autoreactive Façade System for Urban Heat Island Mitigation in Athens, Greece

Christina Koukelli [1,*], Alejandro Prieto [2,*] and Serdar Asut [3,*]

[1] Arup Deutschland GmbH: Joachimsthaler Str. 41, 10623 Berlin, Germany
[2] Architectural Facades & Products Research Group, Department of Architectural Engineering + Technology, Faculty of Architecture and the Built Environment, Delft University of Technology, Julianalaan 134, 2628 BL Delft, The Netherlands
[3] Chair of Design Informatics, Department of Architectural Engineering + Technology, Faculty of Architecture and the Built Environment, Delft University of Technology, Julianalaan 134, 2628 BL Delft, The Netherlands
[*] Correspondence: ckoukelli@hotmail.com (C.K.); A.I.PrietoHoces@tudelft.nl (A.P.); S.Asut@tudelft.nl (S.A.)

Abstract: The paper explores the potentials of shape memory alloys (SMAs) for the design of autoreactive façade systems without using additional external energy. The exploration is conducted and assessed through the design of a façade concept for the city of Athens in Greece, aiming to improve both the indoor and outdoor environment by means of a kinetic autoreactive system featuring a dual-seasonal function, with a focus on the building's direct and indirect impact on the urban heat island (UHI) effect. The paper covers a demonstration of the methodology followed, using a feedback-loop logic informed by environmental and energy performance evaluation studies in Grasshopper to optimize the geometry and movement of the shading component. During the façade design process, a comprehensive and systematic computational toolset is being developed, targeted on the abovementioned performance evaluation studies. Through the development and assessment of the façade concept, the objective is to explore the potentials and limitations for the application of autoreactive envelopes in the façade design. At the same time, the aim is to exploit the possibilities and optimization potentials offered through the developed iterative computational workflows, by showcasing the methodology and interoperability logic of the digital tools used for the data interchange.

Keywords: adaptive; kinetic; dynamic; façade; urban heat island; shape memory alloys; performance-driven design; environmental response; smart materials; computational modeling

1. Introduction

Rapid urbanization during the last decades has had several environmental, economic, and social consequences. Among these, an issue of great concern has been the development of the so-called urban heat island (UHI) phenomenon, characterized by higher temperatures in the density of built areas than the ones of the rural surroundings, which is both directly and indirectly related to serious energy, environmental, health, and economic problems [1]. Apart from that, some other causes include materials with high thermal storage capacity and anthropocentric sources, such as the emissions from air-conditioned buildings, which are related to the building's operational performance. In the European context, this phenomenon is especially intense in the Mediterranean basin, with a fast growth of energy consumption in the last years due to the widespread use of air-conditioning systems and the increase of cooling demand. This situation becomes even

more worrisome in the face of global warming and the significant rise of heat waves (HWs) [2].

Especially in Athens, Greece, UHI has been present already since the 1980s. Research studies have shown that there has been an increase of the energy building demands, thermal risk, and vulnerability of urban population [3–5] and it has been reported that during the HWs, there is even an intensification of the average UHI magnitude by up to 3.5 °C, an outcome of a study reporting the heatwaves in Athens in 2012 [6]. The heat that is dissipated from the buildings to the external environment increases the UHI phenomenon, and, therefore, has a strong indirect impact. More specifically, in Athens, an average increase of the cooling load of about 13% is estimated, with an annual global energy penalty for unit of city surface and degree of UHI intensity of 0.74 kWh m^{-2} K^{-1} [7].

The UHI is a complex phenomenon and is directly and indirectly related to serious energy, environmental, health, and economic problems [3,8]. When it comes to the influence of buildings, it has been established that there is both a direct and an indirect impact of the building's energy performance on the increase of the UHI in the cooling-dominated areas, such as Athens [8]. More specifically, the direct impact which is examined in the current research relates to the reflected solar radiation directed from the building's surface towards the urban microclimate, whereas the indirect one concerns the released heat which is generated from the building's cooling systems and is then accumulated in the urban environment. Other aspects that could also be considered part of the direct impact, such as the infrared thermal transmission due to the surface temperature of external façades, were out of the scope of the current study. An improvement of the building envelope and the energy efficiency might, therefore, reduce the ambient temperature and building's impact and, consequently, decrease the amplitude of the phenomenon.

In this direction, a certain level of climatic responsiveness and adaptiveness to extreme heat changes in an energy-efficient way can arise as a promising strategy, in order to reduce the building's energy consumption. This gives way to the broad development of responsive technologies, such as passive dynamic adaptive façade systems, which are favored due to the real-time responsiveness to the also dynamic and unpredictable environmental changes, acting as the threshold between building and exterior environment. The abovementioned framework is the direction that was followed in the current research study. This was further explored and developed with a focus on the incorporation of smart and shape memory materials (SMMs), such as shape memory alloys (SMAs), by means of a case study in Athens, Greece, and design concept to evaluate their potential for façade application.

In short, shape memory materials (SMMs) belong to the energy-exchanging smart materials and are one of the major elements of intelligent composites because of their unusual properties, such as the shape memory effect (SME), autoreactivity, large recoverable stroke (strain), and adaptive properties which are due to the reversible phase transitions in the materials. More specifically, thermoresponsive SMMs, and SMAs belonging to the same category, can sense thermal stimulus and exhibit actuation or some predetermined response, making it possible to tune some technical parameters such as shape, position, strain, stiffness, and other static and dynamical characteristics [9]. An input of thermal energy alters the microstructure through a crystalline phase change, which enables multiple shapes in relationship to the environmental stimuli [10], making them promising materials for the integration in passive responsive façade applications.

The scope of the current paper was placed on the systematic methodology that was developed for the evaluation of the energy and environmental performance of the proposed façade system and the assessment of its effect in relation to the direct and indirect impact of the building on the UHI effect. However, it should be noted that the focus was placed mostly on the environmental and thermal performance of the proposed system, whereas the visual and indoor comfort were not addressed to a great extent at this stage. These aspects would be part of further and complementary studies and optimizations to

provide a more holistic shading device that would meet all requirements related to building performance and user's comfort.

Based on the above objective, the aim was to address the following main research question:

"What is the potential contribution of an autorective façade system integrating thermo-responsive SMMs to the UHI reduction in the Mediterranean climatic context of Athens?"

2. Materials and Methods

The design methodology was divided into three stages. The first stage consisted of the literature study, where the background information was accumulated to be applied in the design integration, including studies on the material properties and dynamic behavior. After setting a theoretical base, the following stage involved the design phase, which was informed in parallel by research and iterative performance evaluation studies in a feedback-loop process.

In the performance analysis and evaluation stage, computational simulations were implemented to optimize the design. This was assisted by the feedback from the performance validation, to provide design variations in conjunction with energy and environmental simulations throughout the design process. These simulations received the weather and solar radiation data for the region of Athens, Greece (EPW weather data files obtained from the EnergyPlus online database [11]) and attempted a connection to the UHI and its impact on the microclimate and surrounding environment. Besides that, thermal behavior modeling under targeted conditions was realized in a CFD simulation software, as well as energy, radiation, and daylight simulations in different operation periods of the SMM-based shading device. The above iterative process was based on an interoperability toolchain workflow, where most of the digital tools were integrated in the same computational design environment (Grasshopper), transferring data from, and informing, each other in a feedback-loop logic. Figure 1 provides an overview of this toolchain analyzed for the purpose of each analysis study. The different plug-ins (Dragonfly, Ladybug, Honeybee) formed the base of the study analyses, where Dragonfly is able to generate and include urban climate data and conditions, addressing some of the UHI parameters, such as the albedo of materials and anthropogenic heat, which is accomplished with the help of the urban thermodynamic engine Urban Weather Generator [12]. Ladybug was focused on the solar radiation and sun ray trace analysis studies, while Honeybee was also targeted at the energy analysis and energy use intensity calculation. Throughout this data transfer and exchange, additional energy simulation engines were integrated, which were necessary for the processing of the energy simulation runs, such as EnergyPlus [11] and OpenStudio [13], together with Radiance [14], DaySim [15], and THERM [16], which targeted the more specific studies, such as daylight analysis (which was not covered in the current paper) and energy heat flow modeling.

Based on the above workflow, the evaluation methodology consisted of assessing the SMM adaptive façade system's performance, based on the performed energy and environmental simulations. The objective was to estimate the impact of the system on the urban microclimate from the reflection of the solar radiation, as well as the effect on the reduction of the building's cooling demands.
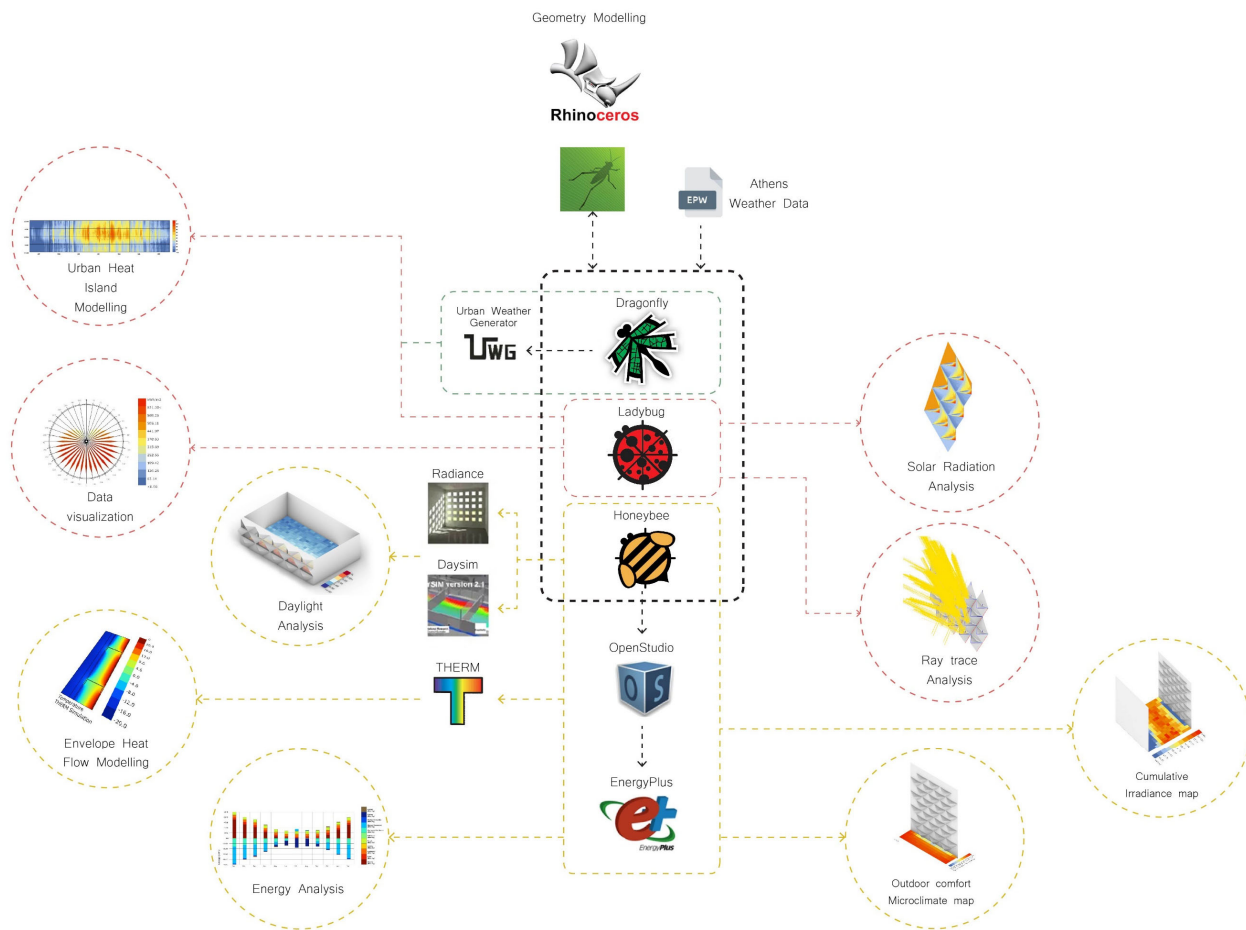
Figure 1. Overview of the digital tools workflow in the Grasshopper environment, highlighting the main plug-ins (Ladybug, Honeybee, Dragonfly) and energy simulation engines (OpenStudio, EnergyPlus, Radiance, DaySim, THERM), as well as the individual study analyses.

The study and evaluation of the performance of the proposed façade design were divided into two stages based on how they address the building's direct and indirect UHI impact, and can be explained as follows:

- The first step was related to the direct UHI impact, which concerned the proportion of sun rays reflected towards the atmosphere, realized in a component, façade segment, and an urban level. This step was influenced mostly by the geometrical features of the component and the arrangement of the façade, considering a horizontal or a vertical arrangement of the component along a façade segment.
- Once a sufficient proportion of the reflected radiation to the atmosphere was achieved (over 75%), the next evaluation criterion concerned the indirect impact, which was related to the building's energy performance, and more specifically, its cooling load demands.

The above stages set the minimum of requirements, which formed the façade guidelines, that would give a design with satisfactory results to provide useful feedback for the performance evaluation and possible further optimization of the façade system. Due to the complexity of the UHI phenomenon, however, more factors were intertwined, for example, the passive operation of the façade mechanism on either a daily or a seasonal basis, as well as the impact of the façade orientation. In an ideal operational scenario, all the requirements would have to be satisfied to achieve an optimal adaptive environmental and energy performance. In practice, though, since the façade design was focused on a

fully passive operation, the above ambition would lead to a mechanism which is too complex and unrealistic to operate. The objective of these feedback-loop workflow and optimization stages was, therefore, to identify the sweet spot where the system is as little complex as possible with minimal presence of mechanical and structural parts, to maximize, at the same time, the building's environmental performance in relation to the UHI effect. The feedback-loop workflow of the direct impact evaluation is shown in Figure 2.

For the scope of the paper, the design concept development is briefly explained to provide the design case example, and more focus is placed on the energy and environmental performance based on the direct and indirect impact evaluation, showcasing the computational workflow and interoperability toolchain logic developed during the process.
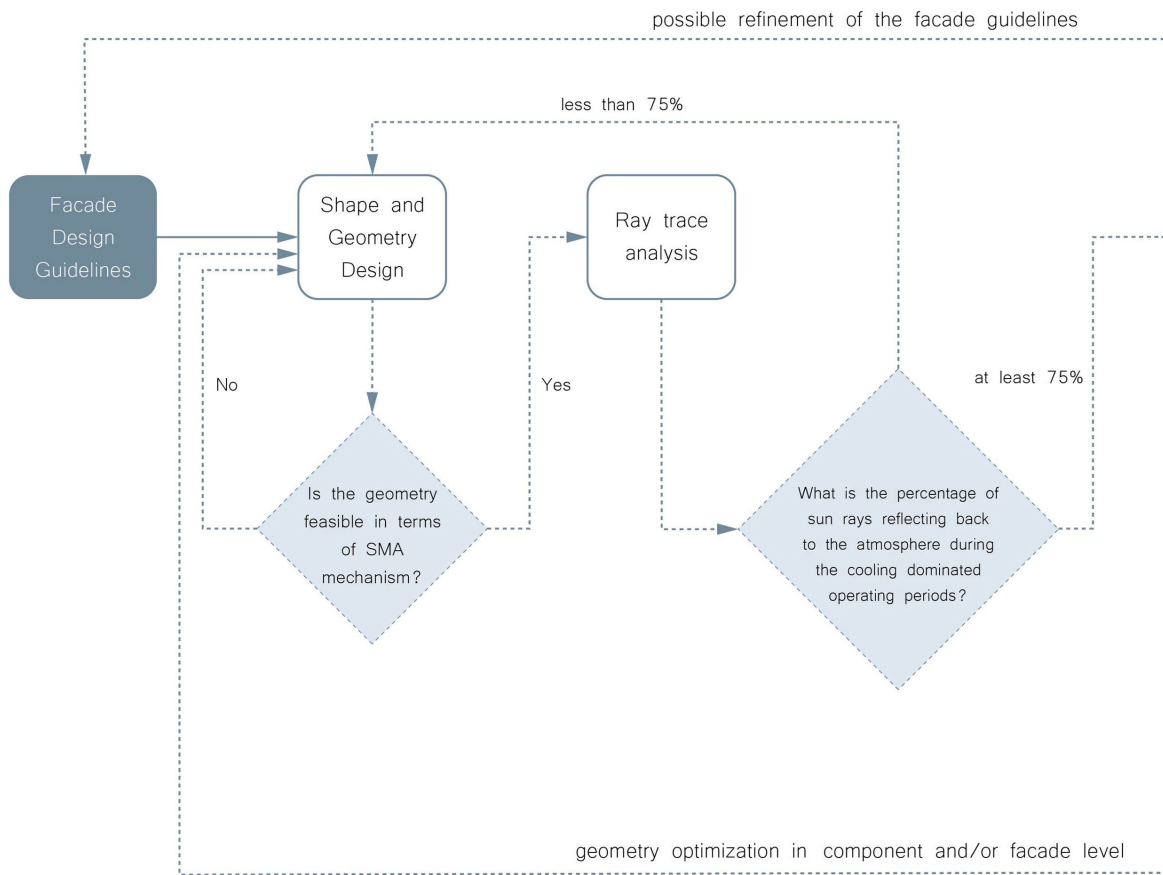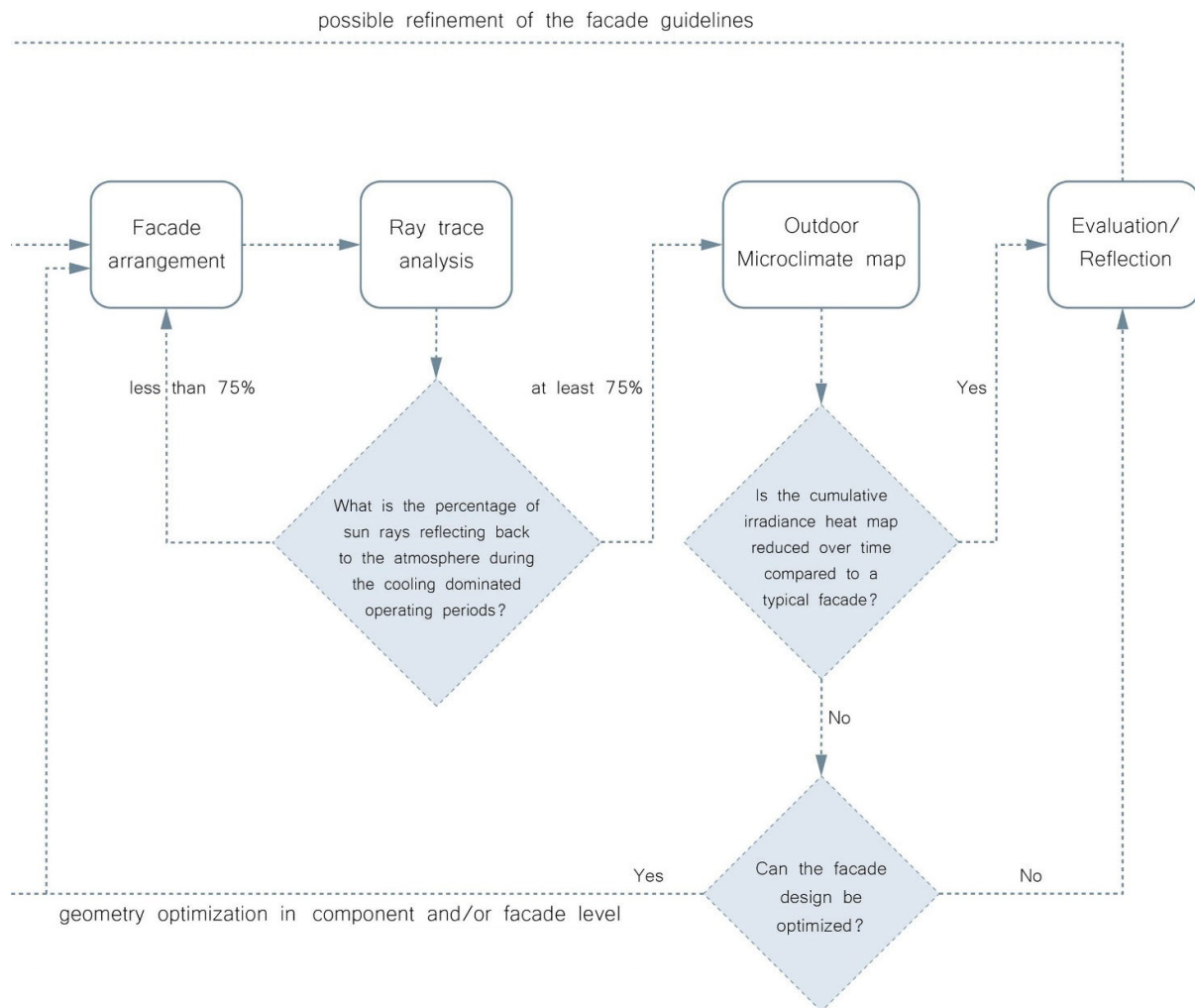
Figure 2. Flowchart of the feedback-loop iterative process of the UHI's direct evaluation workflow.

2.1. Concept Design

The goal of the façade design was to propose a low-energy and low-tech façade system capable of predictably changing in shape in response to temperature changes through the ingrained properties of the material it is made of, without the need for external energy or complex mechanical parts, and by optimizing the use and number of actuators required to achieve the desired result. In this way, by applying the shape memory effect of the material, a control of the thermal transmission of the building envelope can be achieved, as well as a reduction of the thermal transfer through an optimal dynamic performance of the façade skin.

The façade design proposal concerned the development of a self-shading skin integrated in an exterior façade system, aiming to regulate the heat exposure in both the cooling- and heating-dominated periods. The base of the idea was that the envelope structure consists of an inner solar absorbing coating layer and the outer SMM-based shape-morphing skin, which forms a dynamically responsive and reflective articulated surface (Figure 3).
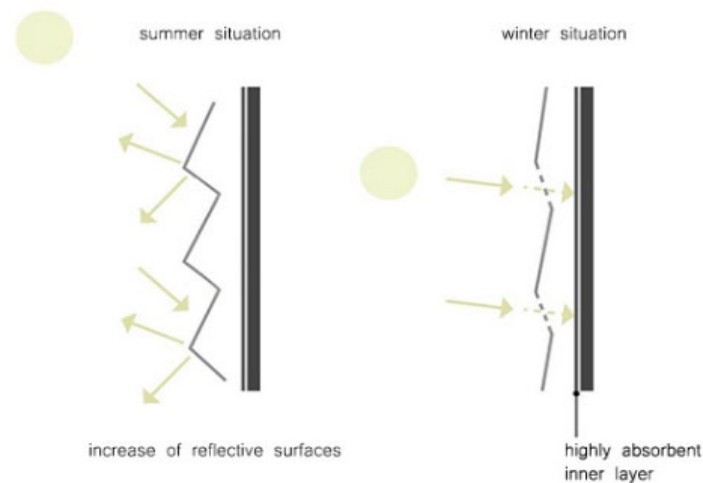
Figure 3. Design concept for the dual-seasonal function.

An important aspect for the energy and environmental performance evaluation of the design was to first establish a set of design goals. These can be divided into the two distinct façade performance operations, during cooling- and heating-dominated periods, and how they address both the direct and indirect UHI impact in each case. This distinction was enabled by the dynamic movement of the façade component, which passively allowed for the dual movement and transition throughout the seasons to adapt to the different heating, ventilation, and shading needs. The goal was to reduce the cooling demands of the building during hot periods and the heating demands during the cold seasons, while minimizing the building's solar radiation reflectivity towards the urban environment throughout the year. However, since a fully automated system might not reach the maximum possible effect, the possibility to override the function could potentially be incorporated as a design option to enable the user's freedom of operational control.

Regarding the summer scenario, the goal was to increase the undulated shading surfaces. By doing so, the self-shading is increased, reducing the direct solar radiation that is absorbed on the façade surface while increasing the number of surfaces that are positioned perpendicular to the solar rays, and reflecting the radiation back to the atmosphere. In relation to the indirect impact, the undulated surfaces also act as primary shading devices that obstruct the direct sunlight to the interior of the building from the south, but also from east-to-west. When it comes to the air cavity function, the goal was to achieve an open-air cavity ventilation that works as a heat attenuation zone, which exhausts and helps circulate the hot air that is accumulated inside, with the skin acting as an independent exterior shading.

The situation is reversed during wintertime, when the increase of the incoming solar radiation is desired to reduce the building's heating demands. To achieve this, the movement was more focused on decreasing the undulated shading surfaces, to admit more sunlight to the interior and to increase the solar radiation, which is being absorbed through the outer surface layer. At the same time, considering the lower position of the sun during the cold months, the top surface, which tracks the sun's seasonal movement, was also lowered to be in a perpendicular position, similarly to the summer situation, and to switch the top side to a more absorbent one in terms of materiality. In accordance with the energy performance, there was an increase of exposed surfaces that can absorb heat, such as the inner glazing or a highly absorbent coating in the opaque building surfaces inside the cavity, in combination with a closed-air cavity ventilation system, which functions as a heat buffer with multiple amplification zones.

The concept development of the final design is illustrated in Figure 4. In principle, two SMAs were positioned on the bottom edges of the bottom pyramid and were connected to a pivot axle connected on its turn at the common edge of the top and bottom parts. The deformation of the SMAs initiated the rotation of the axle, which caused, on one hand, the rotation of the bottom pyramid, and on the other hand, the linear movement of the top part. The two end positions can be seen in Figure 5.
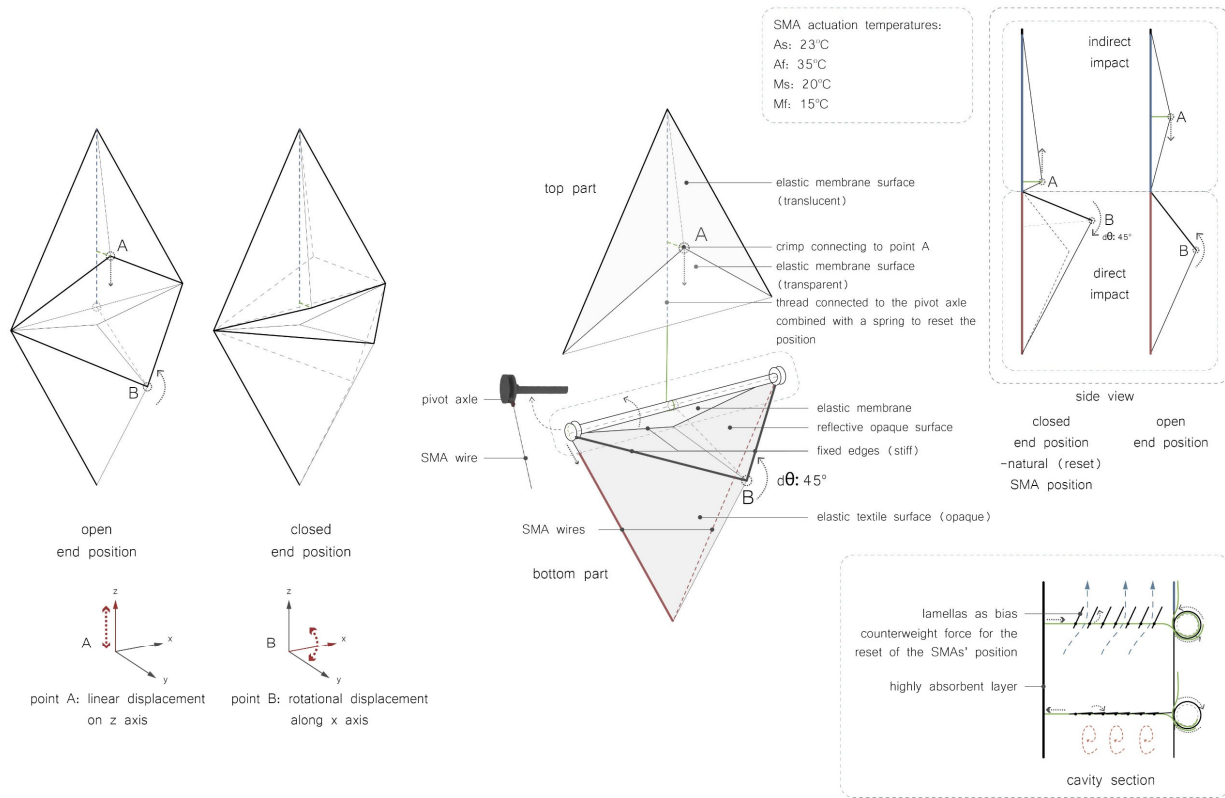

Figure 4. Conceptual sketches illustrating the SMA operating mechanism and components.

summer situation

winter situation

ETFE single-layer translucent membrane

deployable ETFE single-layer transparent membrane

PTFE coated fiberglass ventilated open mesh (stretched)

PTFE coated fiberglass ventilated open mesh (closed vents)

top mechanism zoom-in

top mechanism zoom-in

lamellas in open position

bias spring
bullet terminal connector attached to textile
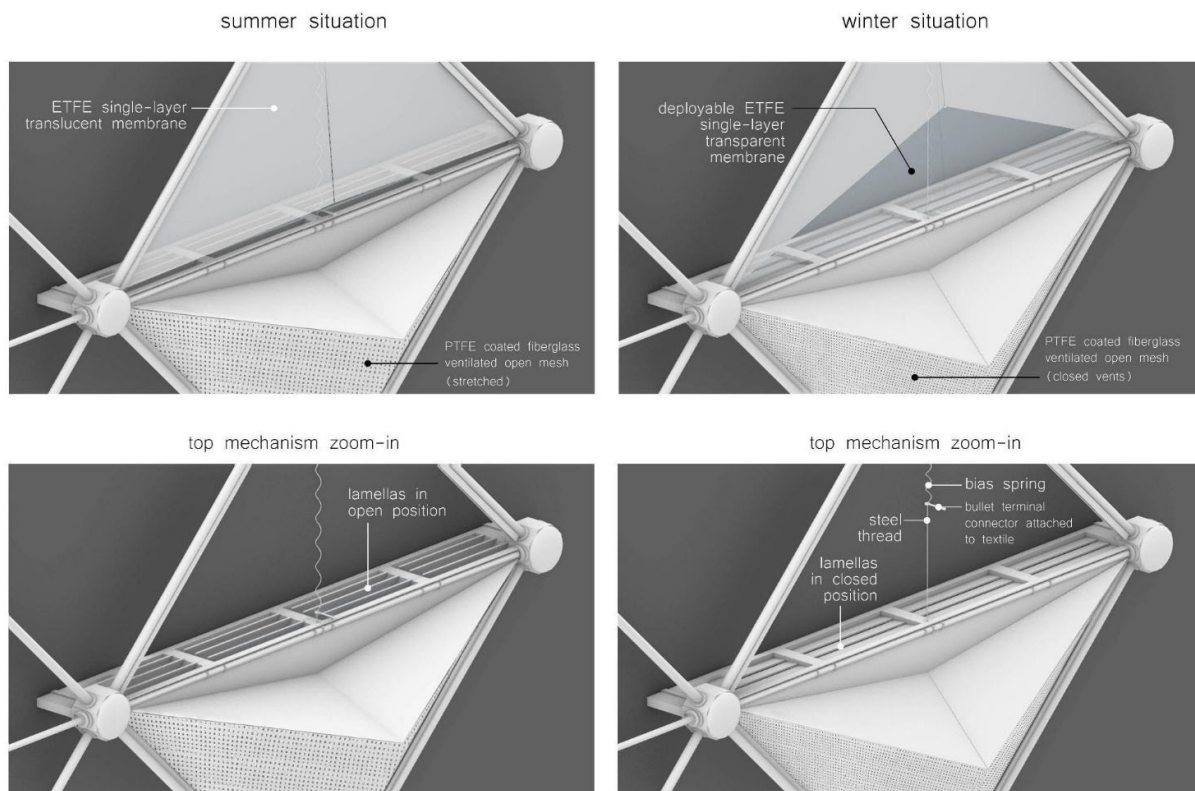steel thread
lamellas in closed position

Figure 5. Close-up views of the façade component and mechanism during the summer and winter situation.

2.2. UHI Direct Impact Evaluation

2.2.1. Sun Ray Trace Analysis Studies—Component and Façade Level

The first explorations of the initial geometry concept were based on the proportions of the component and how these relate to their environmental performance in terms of solar radiation, to receive a first indication on the impact of the self-shading effect and how the proportions affect the overall scale and performance, as seen on the figure below (Figure 6). However, since the most important factor to evaluate the direct impact was the reflectivity of the sun rays back to the atmosphere, a first round of sun ray trace analyses on a segment of the façade was realized. The first results already showed that the original geometry reflected only about 10% of the rays. This was mostly due to the rays reflected from the top pyramid downwards, and led to a geometry refinement, having a more flattened pyramid on top. Apart from that, the rotation of the bottom pyramid was optimized to have the top surface perpendicular to the sun rays from June to December as a first case (Figure 7).
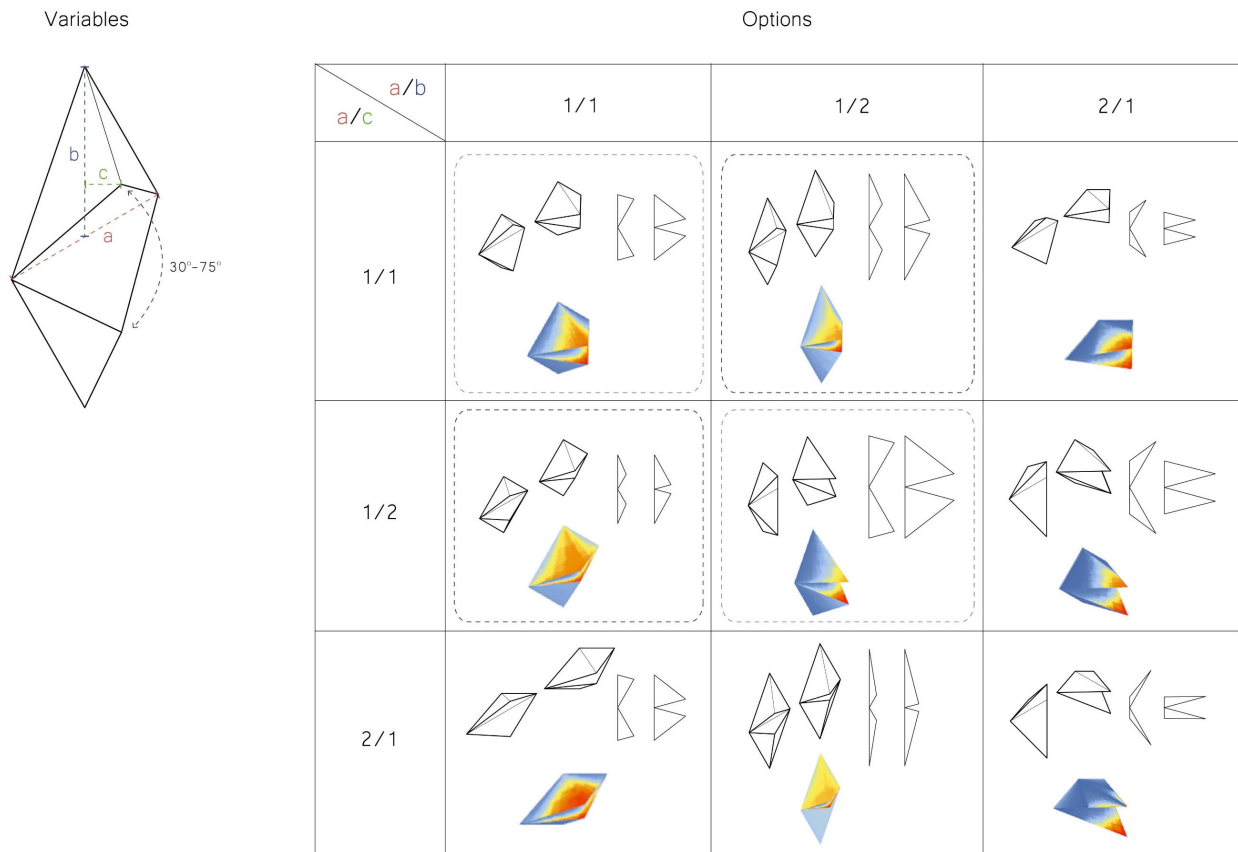
Variables

Options

a/b — a/c	1/1	1/2	2/1
1/1			
1/2			
2/1			

Figure 6. Overview of the various geometry alternatives based on proportions and sizes and a first solar radiation study.

reflected rays above bounce surface:
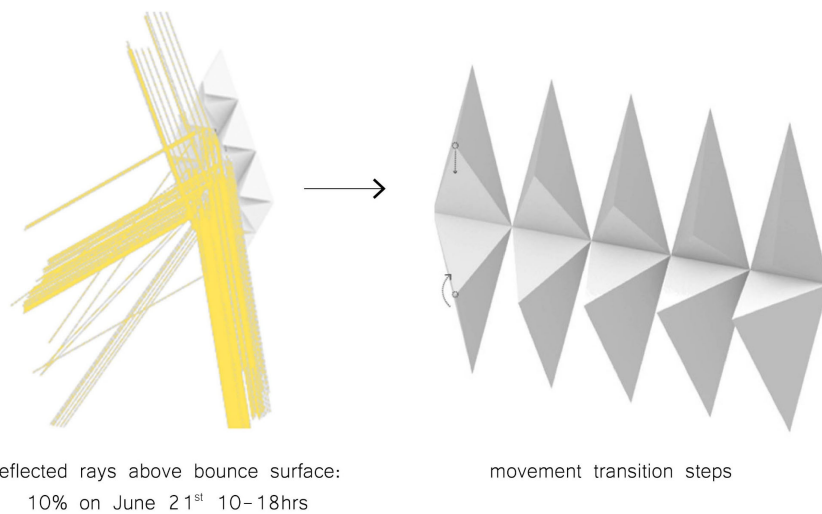10% on June 21st 10–18hrs

movement transition steps

Figure 7. Overview of the various geometry alternatives based on proportions and sizes and a first solar radiation study.

During the ray trace analysis, a backward ray-tracing method was followed using a combination of a forward ray trace analysis and the "Bounce from Surface" component of

the Honeybee plug-in. The advantage of the latter method is that it also enables the visualization of the sun rays after several bounces, considering the rays reflected from the neighboring surfaces before bouncing off to the atmosphere or the urban environment. In this study, the analysis considered 2–3 bounces and evaluated the reflectance both between the different proportions and between a horizontal and a diagonal arrangement. A summary of the results can be found in Figure 8, where it was concluded that Option 2 showed a good enough performance with both a larger rotational range with a starting angle between 45°–50° and a strain ratio within allowable limits of 3–5% strain. Some further observations were the existence of a "blind" angle, which corresponds to the rays being reflected from the top pyramid downwards through the in-between geometry gaps in certain time periods, as also seen in the diagram below. The analyses showed that the bottom pyramid's size and arrangement had the most impact on obstructing the sun rays from the top ones with a wider geometry being more efficient towards this goal. In this respect, the diagonal façade arrangement exhibited a better performance as well, because those rays were reflected back to the atmosphere by the neighboring components and the ones below, as a result of the more scattered component distribution, while the horizontal one had a negligible impact. These observations led to the final refinement set of component proportions for each pyramid to be used for the next studies, which were length-to-height: 1/0.5 and base-length-to-pyramid-height: 1/0.5, with an overall component proportion of 1/1.
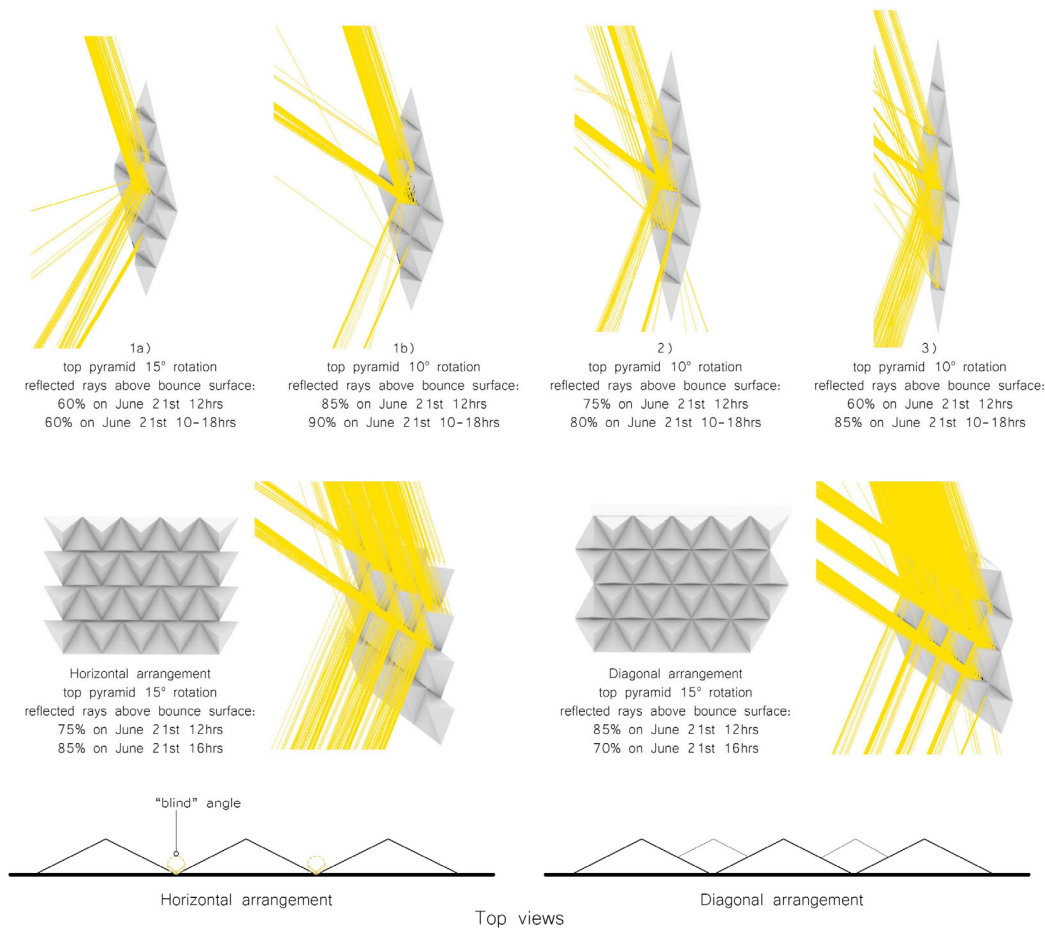

Figure 8. Top: Summary of the sun ray trace analysis studies and in comparison to the façade arrangement. **Bottom**: The impact of the "blind" angle impact and the difference between the horizontal and diagonal arrangement.

2.2.2. Outdoor Microclimate Studies—Urban Level

Cumulative Irradiance Heat Maps

Following the component level, the stage of evaluation of the direct UHI impact on the urban level involved the simulation and visualization of the cumulative irradiance on the urban environment, assuming the scenario of an urban street canyon in Athens with the proposed south-oriented façade design. The most important part of this study laid on quantifying the reflected part of the solar energy and assessing the effect of the façade geometry on its reduction on the street level and the neighboring buildings, in comparison to a typical façade surface, different surface types, and window-to-wall ratios.

For this study, two approaches were followed, in accordance with the design tool's possibilities. In the first case, the Honeybee Daylight Analysis component was used to calculate the cumulative irradiance on the street level, which accounts for direct, diffuse, horizontal infrared, and reflected solar radiation from the surrounding surfaces. In this case, it was also possible to include information of the surface types, ranging from fully absorbent (R:0, G:0, B:0) to fully reflective ones (R:1, G:1, B:1), and the glazing ratio, comparing a fully opaque (0%) to a curtain wall (85%). However, it was not possible at this early design stage to insert and consider more detailed material inputs and properties. The analysis was conducted for the extremely hot week (03–09/08) as the worst-case scenario.

However, even though the first methodological approach provided an indication of the cumulative radiation on the street level, the distinction between the different types of radiation and the contribution of the reflected part was not entirely clear. For a more comprehensive understanding, a complementary approach was followed, using the Ladybug Radiation Analysis component this time. The difference in this case was that the radiation accounts only for the direct and diffuse radiation (the infrared radiation is included by default in both cases). By decoupling these two analyses, it could then be possible to extract the value of the reflected radiation and compare the results, allowing for small divergence in the values due to possible slight differences in the two calculation processes. The flowcharts of the workflow for these two approaches are illustrated in Figure 9.
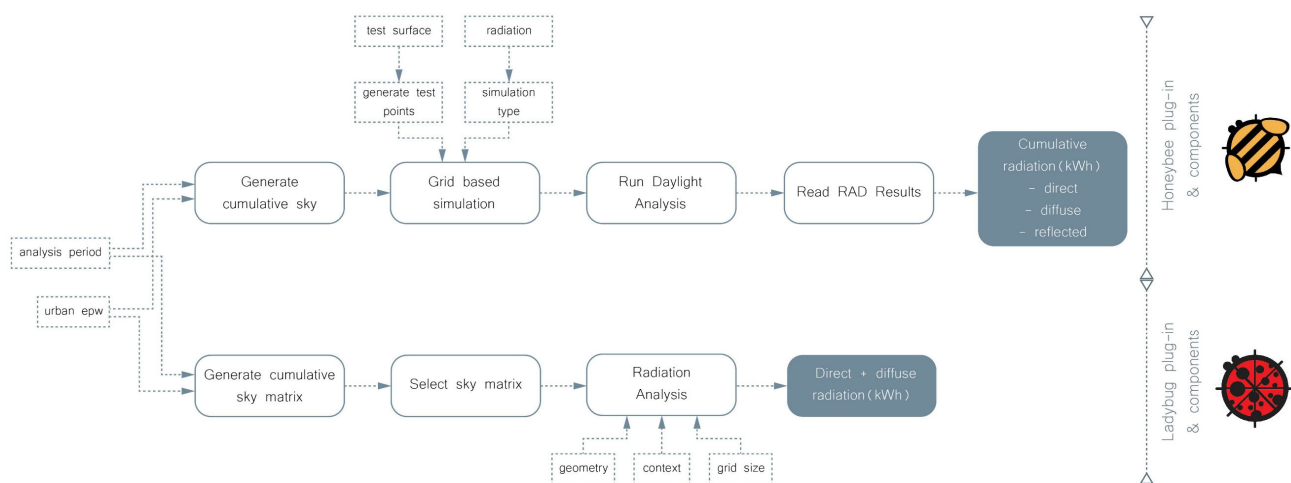

Figure 9. Flowchart of the two workflow approaches for the radiation analysis study and the design tools used for each case.

Comparative Sun Ray Trace Analyses

Lastly, a final validation check on the direct environmental impact of the façade was conducted in relation to the direction of the reflected sun rays as a full building façade and not as an isolated component or segment, and in the context of the urban street canyon

with surrounding buildings opposite to the analyzed one. Since the façade is south-oriented, the study concerned only the rays reflected from the proposed façade to the surroundings and not from the opposite-facing building. The analysis considered the date of 21 June between 12:00–13:00, when the sun is at its highest peak, and the comparison was then realized between the current design and a typical flat façade.

2.3. UHI Indirect Impact Evaluation—Building's Energy Performance Evaluation Studies

As previously explained, the UHI indirect impact evaluation relates to the building's energy performance, as well as the effect of the façade skin and the cavity function primarily on the reduction of the cooling loads and, consequently, also on the inner comfort.

For the evaluation process, the studies were focused mostly on the dual-cavity function in the cooling- and heating-dominated periods, to simulate the dynamic air and heat flows throughout the day and to visualize the temperature fluctuations through the cavity section to the interior. For these purposes, the studies were divided into analyzing the summer and winter situation, with the summer one to be the most critical one for the evaluation of the proposed façade system on the indirect impact, and the winter one to work more as a validation control and understanding of the proposal for the cavity function. During the summer scenario, the focus was placed on estimating the cooling demands and assessing the parameters and boundary conditions that influence the performance and, in the end, comparing the results to the existing single façade scenario. On the contrary, for the winter situation, it was more insightful to simulate the heat and air flows inside the closed cavity zones and to visualize the temperature fluctuations from the exterior to the interior of the building to assess the effect of the thermal heat buffer zones and to make a comparison with different boundary conditions and cavity widths. Finally, as a side study, a daylight analysis was conducted to evaluate the shading effect in the interior of the building with different component scales, to what extent the inner comfort is affected, and the percentage of reduction of the admitted daylight, in relation to the existing façade with no external sun-shading.

The study workflow for these analyses can be seen in the flowchart below (Figure 10). The approach followed an interoperability and decoupling method, due to software limitations and to exploit the possibilities of the most suitable software for the requirements of each study. More specifically, for the cooling demands analysis, the Honeybee plug-in in Grasshopper was used, which enables the simulation of the different thermal zones, internal loads, and ventilation options and can provide an estimation of the energy use intensity (EUI) indicator for the analyzed periods. Since it is an early design stage, this approach provided sufficient and accurate enough results to give a first indication of the building's energy performance.
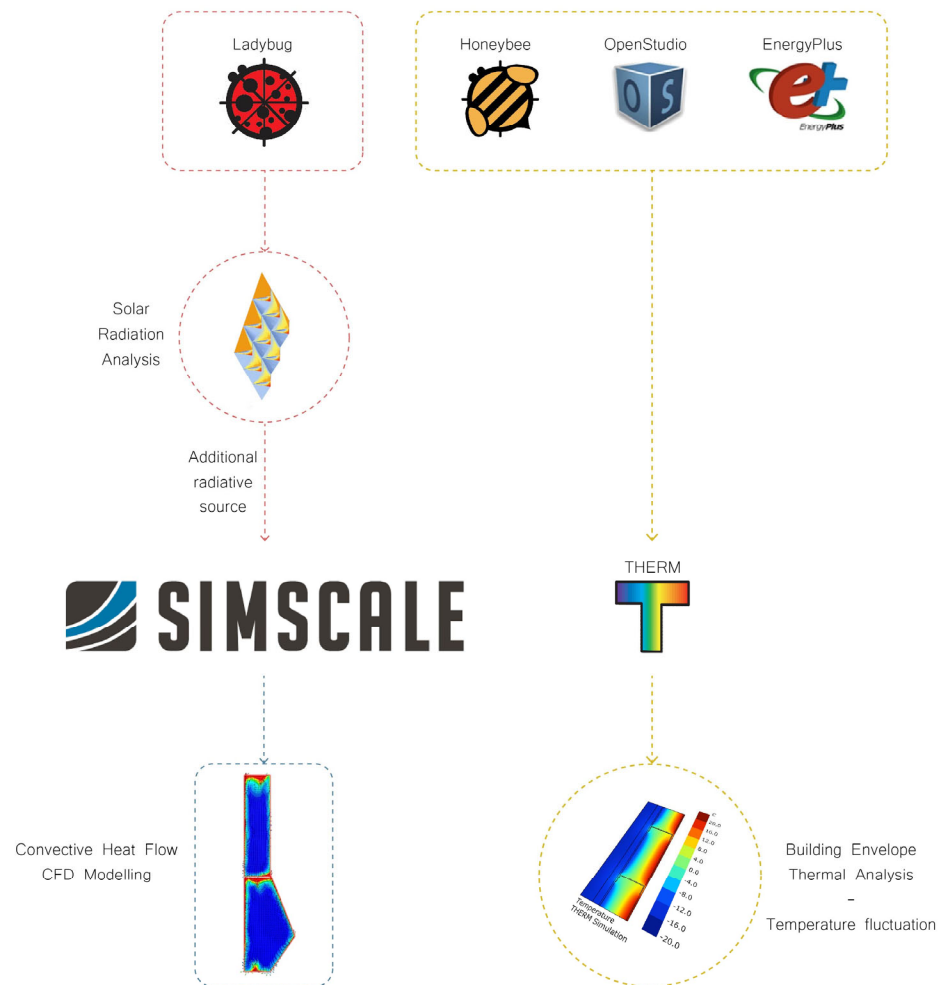
Figure 10. Overview of the toolchain and the data interchange between the different design tools used for the thermal simulation studies.

In parallel, since the cavity system functions in a more dynamic way, CFD simulations were also necessary. These were realized using the open-source online digital software SimScale [17], which could be compatible with geometries imported from Rhino, and, without necessarily requiring extensive experience in fluid dynamics and CFD modeling, it can provide satisfactory, yet with certain simplifications, results. This method was coupled with data provided by the Ladybug radiation analysis, which was used to retrieve the solar radiation value to be assigned as an additional radiation heat flux (W/m²) on the façade surface for one day. The SimScale simulations were used to visualize the full height cavity flows during the summer situation and the impact of air inlets and outlets, but mostly to also visualize the winter cavity system.

Finally, for the winter situation and as a complementary analysis, the THERM plug-in in Grasshopper was also used, which can provide the temperature fluctuations from the outside to the inside boundary, by selecting material properties and boundary conditions, including the layer behind the cavity zone. Even though it is not a dynamic simulation, it could still provide sufficient results for a specific date and time condition.

2.3.1. Cooling Demands Estimation Studies—Energy Use Intensity (EUI) Indicator

The conclusions from both the direct impact evaluation and the background literature research have indicated that the building's energy performance and the indirect impact of the cooling systems eventually have a stronger effect on the UHI intensification. In this section, studies on the energy use intensity (EUI) indicator were realized to estimate the cooling demands per area in different scenarios and ventilation strategies of the proposed façade system and compared to the existing case study office building as a benchmark condition. The studies were focused on the cooling-dominated periods (April–October) of the façade system's operating schedule, with a focus on the summer peak.

The workflow followed is explained in the flowchart below (Figure 11) and, during the methodology, the Honeybee plug-in was used in combination with the integrated Energy Simulation engines EnergyPlus and OpenStudio. Due to some limitations of the software and the way the processing functions, certain simplifications were applied, which, however, had a negligible effect on the validity of the results. For example, the geometry needed to be slightly simplified to enable surface adjacencies and to avoid simulation errors when translating the geometries to the different boundary thermal zones. Another simplification included the solar distribution to only account for the exterior direct and blocked solar calculation, with the beam solar radiation to be assumed to fall on the floor without considering the interior reflections. This was due to the presence of convex geometries, which cause errors during the interior solar calculation, because of the many reflecting angles.
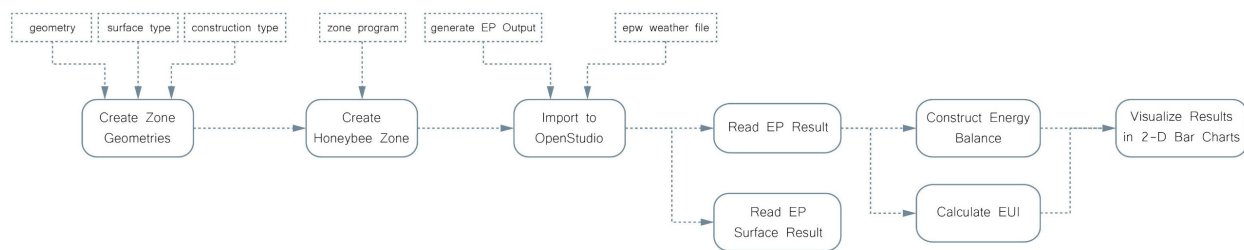

Figure 11. Flowchart of the energy use intensity calculation workflow.

Additionally, one floor of the building was taken as the test geometry with dimensions of 10 m (façade length) × 6 m (room depth) × 3 m (floor-to-ceiling height), which was divided into two thermal zones, the interior with the inner layer as one, and the cavity zone with the outer layer as a second one. For the purposes of the current study, an inner façade with 60% window-to-wall ratio was assumed as a base case scenario for the analyses. The outer boundaries of the interior were considered as adiabatic surfaces, whereas the inner layer, which was the interface between the interior and the cavity, was assigned as an "Air Wall", which in EnergyPlus is translated as enabling the air and heat exchange between the two zones [11]. The influence of this setting, however, was also tested in the following simulation cases to evaluate the different ventilation and air flow scenarios. Apart from that, the boundaries of the cavity zone were also assigned to be adiabatic and the outer façade layer, which involves the proposed design, was set to be an exterior boundary. The cavity was assigned as an unconditioned plenum zone and as a default dimension; it was assumed to be 400 mm wide, which was a measurement proven to have efficient air and heat flow performance in double façade systems, based on literature research [18], however, this was also chosen as a variable to be used for validity check. Lastly, since materiality had a meaningful role in the amount of solar radiation admitted to the interior, in relation to the properties of the opaque, but mostly the translucent, textile part of the exterior layer, the specific energy performance values were also assigned to the corresponding materials. Here, also, the option to adjust and assess various alternatives for the translucent part was left open, to explore the solar control possibilities with

low-e integrated coatings or fritted patterns and different solar heat gain coefficient (SHGC) values, and their impact on the reduction of the cooling loads.

The input parameters for the evaluation studies can be seen in the overview figure below (Figure 12), including the interior and boundary conditions and the setups for air flow, internal loads, and material properties, with a cooling setpoint at 24 °C and a heating setpoint at 15 °C [19–22]. The inputs highlighted in red are considered as variables.
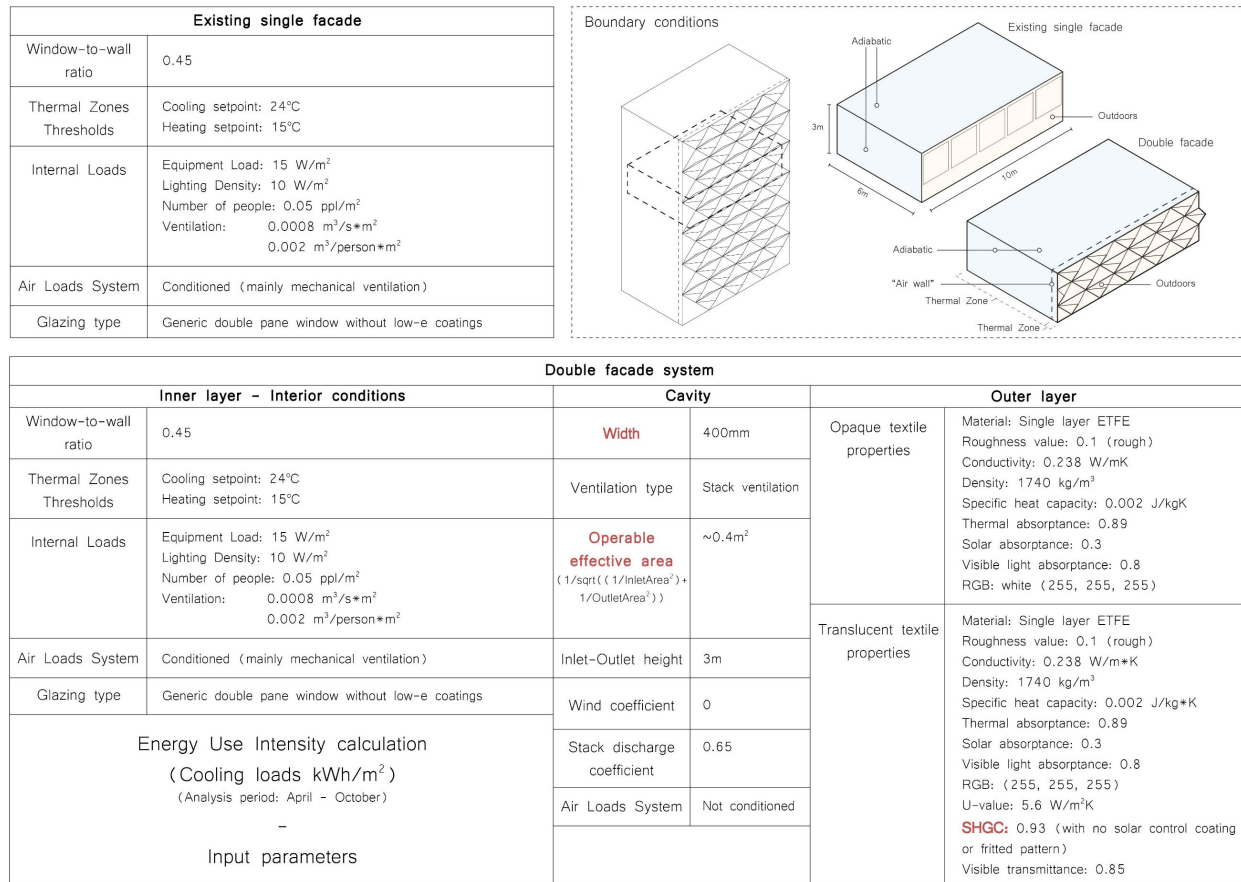
Existing single facade	
Window-to-wall ratio	0.45
Thermal Zones Thresholds	Cooling setpoint: 24°C Heating setpoint: 15°C
Internal Loads	Equipment Load: 15 W/m² Lighting Density: 10 W/m² Number of people: 0.05 ppl/m² Ventilation: 0.0008 m³/s∗m² 0.002 m³/person∗m²
Air Loads System	Conditioned (mainly mechanical ventilation)
Glazing type	Generic double pane window without low-e coatings

Double facade system					
Inner layer – Interior conditions		**Cavity**		**Outer layer**	
Window-to-wall ratio	0.45	Width	400mm	Opaque textile properties	Material: Single layer ETFE Roughness value: 0.1 (rough) Conductivity: 0.238 W/mK Density: 1740 kg/m³ Specific heat capacity: 0.002 J/kgK Thermal absorptance: 0.89 Solar absorptance: 0.3 Visible light absorptance: 0.8 RGB: white (255, 255, 255)
Thermal Zones Thresholds	Cooling setpoint: 24°C Heating setpoint: 15°C	Ventilation type	Stack ventilation		
Internal Loads	Equipment Load: 15 W/m² Lighting Density: 10 W/m² Number of people: 0.05 ppl/m² Ventilation: 0.0008 m³/s∗m² 0.002 m³/person∗m²	Operable effective area (1/sqrt((1/InletArea²)+1/OutletArea²))	~0.4m²	Translucent textile properties	Material: Single layer ETFE Roughness value: 0.1 (rough) Conductivity: 0.238 W/m∗K Density: 1740 kg/m³ Specific heat capacity: 0.002 J/kg∗K Thermal absorptance: 0.89 Solar absorptance: 0.3 Visible light absorptance: 0.8 RGB: (255, 255, 255) U-value: 5.6 W/m²K SHGC: 0.93 (with no solar control coating or fritted pattern) Visible transmittance: 0.85
Air Loads System	Conditioned (mainly mechanical ventilation)	Inlet-Outlet height	3m		
Glazing type	Generic double pane window without low-e coatings	Wind coefficient	0		
Energy Use Intensity calculation (Cooling loads kWh/m²) (Analysis period: April – October) – Input parameters		Stack discharge coefficient	0.65		
		Air Loads System	Not conditioned		

Figure 12. Overview of the input parameters and boundary conditions for the energy use intensity calculation.

2.3.2. Thermal Analysis—Heat and Air Flows Simulations

In parallel to the assessment of the cooling demands, thermal analyses were conducted to simulate and visualize the heat and air flows inside the cavity and to obtain an approximation of the temperature fluctuations between the outside and the interior boundary zones.

As explained before, for these studies, an interoperable decoupling methodology was followed, combining radiation analysis and temperature surface output data through Ladybug plug-in to be used as input of the additional radiative sources for the SimScale convective heat transfer simulations. In this way, the convective and radiation heat transfer could be solved with the absorbed solar radiation treated as a heating source on the façade skin surface. This is a compromised alternative due to the difficulty in accurately modeling the radiation heat transfer and the complex nature of this type of analysis. By using EnergyPlus to solve the radiation heat transfer, this step can provide surface temperatures and heat flux values under certain weather conditions to be assigned in the CFD simulation as boundary conditions. The CFD simulation can then return the air temperature distribution and the corrected convective heat transfer coefficient, as well as airflow

rates in the cavity, to update the heat transfer calculation by EnergyPlus. This decoupling method has been proved to be effective in predicting the thermal behavior of double skin façades and has already been tested in similar research projects [23–25]. A similar approach was, therefore, also followed in the current study.

At the same time, the results from SimScale were compared to the static temperature fluctuations calculated in the THERM plug-in and software environment. Even though the two approaches follow a slightly different process information logic, and the thermal analysis in THERM does not include air flows, it helped as a complementary study to understand the temperature fluctuations, including the building envelope behind the cavity, and to give an indication of the thermal buffer effect of the cavity during the winter. Apart from that, it was also possible to assign additional material properties as inputs and in the end during the comparison of the two workflows, to complement each other and compensate for their possible limitations. The workflow, input parameters, and boundary conditions for the THERM simulation are summarized in the flowchart in Figure 13 and the overview in Figure 14.
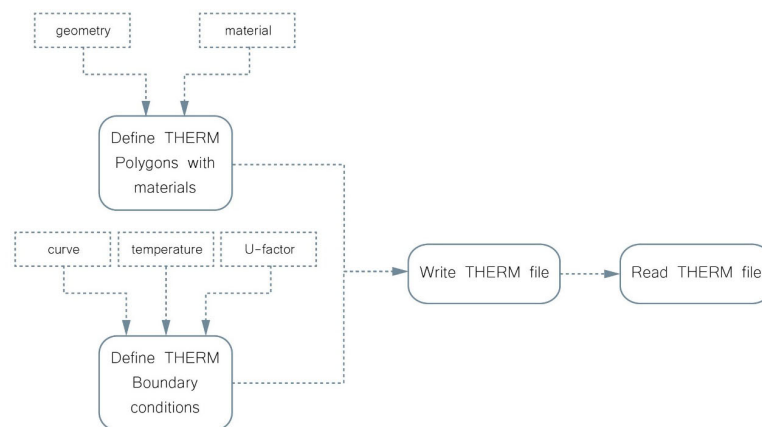
Figure 13. Flowchart of the workflow for the THERM analysis.

As for the SimScale simulation setup, a steady-state convective heat transfer analysis was realized for a duration of 3600 s. This time duration, however, led to certain limitations, because it still simulated a fragmented time frame and could not show the full cavity function throughout a whole day, which would then cause an increase in computational time. The input geometries imported from Rhino were also simplified to be easily translated as one closed volume that was used for the air flow, where only the interior boundary surfaces were modeled. For example, the surfaces needed to be continuous and not intersecting, so areas where the multiple cavity zones were positioned needed to leave a small gap and not be fully sealed. Another limitation concerns the applied additional radiation heat, which was assigned as one average value distributed homogeneously on the outer boundary surface, whereas during the solar radiation analysis it was mostly concentrated on the top surface of the bottom pyramid, which was more exposed to the direct sunlight.
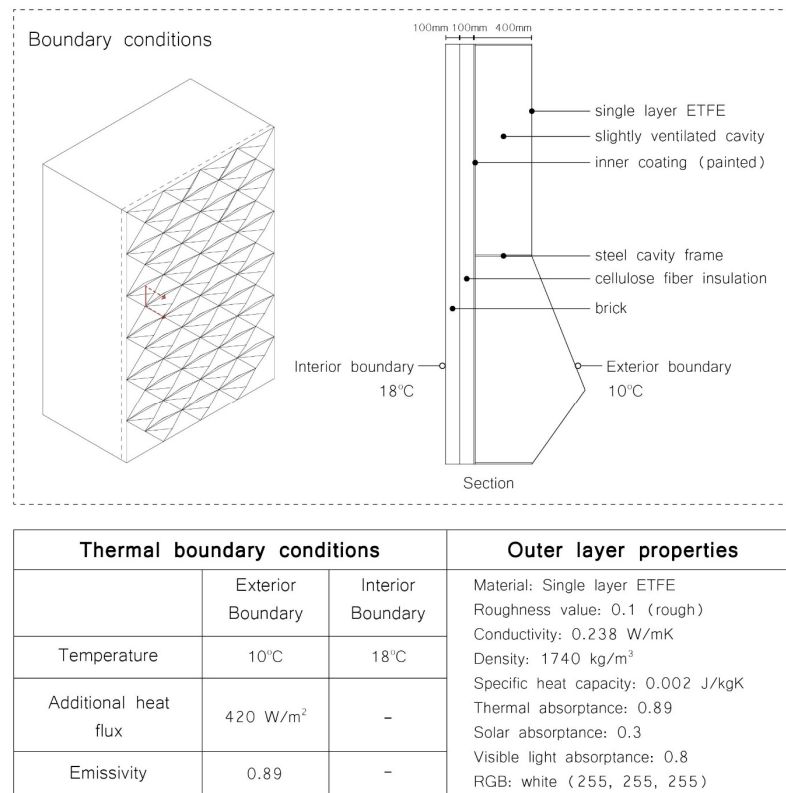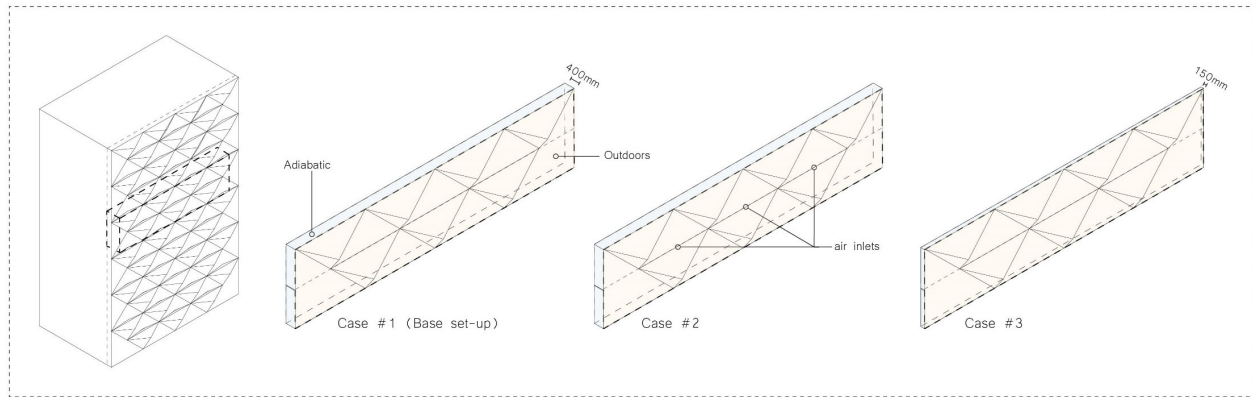
Figure 14. Overview of the input parameters and boundary conditions for the THERM analysis.

The simulation runs were grouped into the two seasonal scenarios, summer and winter, with sub-cases in each situation. In the winter scenario, with an ambient temperature of 10 °C and a surface temperature of 13 °C (data retrieved from the Annual Weather and Radiation analyses), the interest was placed on the heat accumulation inside the multiple cavity zones, the increase in temperature that is caused due to the heat stack effect and the impact of the cavity width, as well as to visualize whether the interior volume of the pyramid worked indeed as a heat convection zone. The case studies in this setup included one floor with two closed cavity zones, excluding the inner building, since there is no air exchange between the two thermal zones. Case#1 was the basic setup with a 400 mm wide cavity and no air inlets or outlets as an ideal scenario, merely functioning as a heat amplification zone, Case#2 featured slight openings through small vents to evaluate the more realistic situation, and in Case#3, a narrower cavity of 150 mm was examined. In practice, there are certain differences in the amount of air inflow, which meant that certain divergence in the simulated results and reality was expected and taken into account.

On the contrary, the summer scenario, with an ambient outdoor temperature of 35 °C and a surface temperature of 31 °C (data from the Annual Weather and Radiation analyses), was modeled as a full height open cavity in the six-story building with a top outlet and the cases were related to the ventilation strategies explored in the previous section. Case#1 allowed air inlets from the outer layer and enabled the air exchange with the interior through air outlets, Case#2 reduced the air flow to only air inlets and flow through the cavity to the top exhaust outlet, and Case#3 investigated the effect of an only slightly ventilated cavity and a top outlet. The summer scenario was focused mostly on the air and heat flows in relation to the impact of the different ventilation strategies on the air circulation inside the cavity.
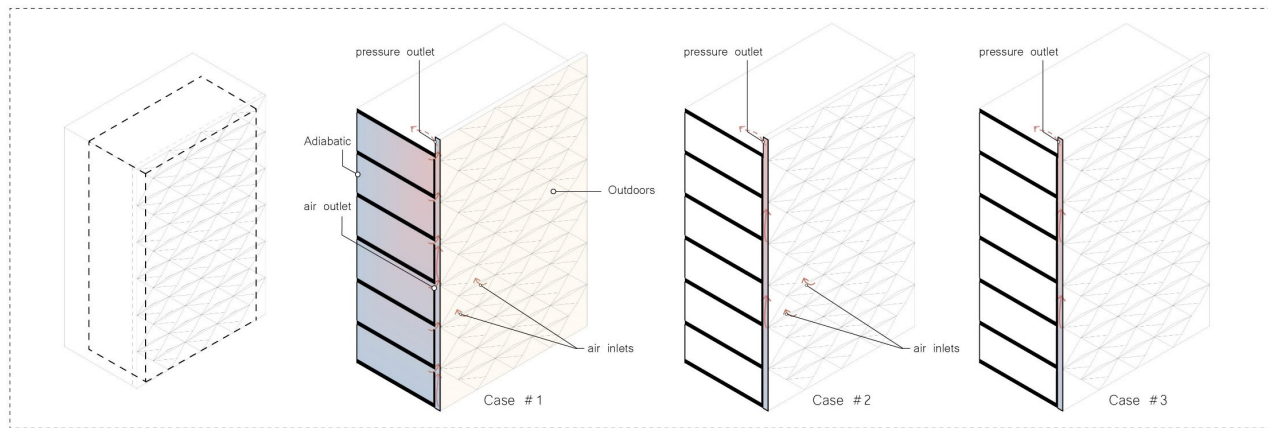
In all the cases mentioned above, the outer layer was considered as an exterior boundary, while the cavity and interior surfaces were assigned an adiabatic boundary condition.

An overview of the initial and boundary conditions for both the summer and the winter situation can be found in the following figures (Figures 15 and 16).

Initial conditions	Boundary conditions			
	Outer layer		Cavity sides – Inner layer	
Fluid: Air Kinematic viscocity: 1.529e-5 m²/s Density: 1.196 kg/m³ Thermal expansion coefficient: 3.43e-3 1/K Specific heat: 1004 J/(kg∗K) Gravity: -9.81 m/s² Global temperature: 10℃ Velocity: 0 m/s	Cavity width	400mm	Temperature type	Adiabatic
	Temperature type	External wall heat flux	Radiative behaviour	Opaque
	Heat transfer coefficient	5.6 W/m²K	Emissivity	0.9
	Ambient temperature	10℃ [value from Annual Weather Data]	Winter situation (Analysis day: 21/12) – Multiple closed-air cavities system	
	Thermal conductivity	0.89		
Simulation control	Layer thickness	12.5mm		
Convective Heat Transfer simulation analysis Time dependency: Steady-state End time: 3600s Time step: 1s	Initial boundary temperature	13℃ [surface temperature value from Solar Radiation analysis]		
	Radiative behaviour	Transparent		
	Additional radiative source	420 W/m² [value from daily Solar Radiation analysis on the facade surface on 21/12]		

Figure 15. Overview of the input parameters and boundary conditions for the SimScale CFD convective heat transfer analysis in the winter situation.

Initial conditions	Boundary conditions				
	Outer layer			Cavity sides – Inner layer	
Fluid: Air Kinematic viscocity: 1.529e-5 m²/s Density: 1.196 kg/m³ Thermal expansion coefficient: 3.43e-3 1/K Specific heat: 1004 J/(kg∗K) Gravity: -9.81 m/s² Global temperature: 35℃ Velocity: 0 m/s	Cavity width	400mm		Temperature type	Adiabatic
	Temperature type	External wall heat flux		Radiative behaviour	Opaque
	Heat transfer coefficient	5.6 W/m²K		Emissivity	0.9
	Ambient temperature	10℃ [value from Annual Weather Data]		Summer situation (Analysis day: 29/06) – Opened-air cavity system	
	Thermal conductivity	0.89			
Simulation control	Layer thickness	12.5mm			
Convective Heat Transfer simulation analysis Time dependency: Steady-state End time: 3600s Time step: 1s	Initial boundary temperature	31℃ [surface temperature value from Solar Radiation analysis]			
	Radiative behaviour	Transparent			
	Additional radiative source	160 W/m² [value from daily Solar Radiation analysis on the facade surface on 29/06]			

Figure 16. Overview of the input parameters and boundary conditions for the SimScale CFD convective heat transfer analysis in the summer situation.

3. Results

3.1. UHI Direct Impact Evaluation—Outdoor Microclimate Studies

The results from the cumulative irradiance maps can be seen in the overview in Figure 17, where with highly absorbent surfaces there was negligible impact between the façade types, since most of the radiation is absorbed and is irrelevant to the façade geometry. This case, however, would lead to undesired effects on the overheating of the building's interior and, thus, increasing the resulting indirect impact. On the other hand, when reflective surfaces were involved, the proposed design's impact was slightly more apparent, but still showed a mere 3% reduction of the total radiation. Perhaps more important was that the radiation was reduced mostly near the façade surface, avoiding unpleasant comfort situations for pedestrians walking nearby. A further aspect concerns also the impact of the façade surface temperature on the UHI effect and the relation between the different surface types, window-to-wall ratios, and cumulative irradiance on the urban environment.

Facade type	Standard facade		Facade design	Observations / Difference in %
Glazing ratio / Diffuse reflectance	0% fully opaque	85% curtain wall		
	Top view grid results			
R:0 G:0 B:0 highly absorbent surfaces	KWh/m2: 51.79<, 50.61, 49.43, 48.25, 47.07, 45.90, 44.72, 43.54, 42.36, 41.18, <40.00 — total: 10540 kWh	KWh/m2: 52.74<, 51.47, 50.19, 48.92, 47.64, 46.37, 45.10, 43.82, 42.55, 41.27, <40.00 — total: 10548 kWh	KWh/m2: 53.43<, 52.09, 50.74, 49.40, 48.06, 46.72, 45.37, 44.03, 42.69, 41.34, <40.00 — total: 10620 kWh	– negligible impact – reflected radiation reduced due to low material diffuse reflectance factors, large part of heat is being absorbed
R:1 G:1 B:1 highly reflective surfaces	KWh/m2: 54.95<, 53.46, 51.97, 50.47, 48.98, 47.48, 45.98, 44.49, 42.99, 41.50, <40.00 — total: 11567 kWh	KWh/m2: 56.11<, 54.50, 52.89, 51.28, 49.67, 48.06, 46.44, 44.83, 43.22, 41.61, <40.00 — total: 11570 kWh	KWh/m2: 53.95<, 52.56, 51.16, 49.77, 48.37, 46.98, 45.58, 44.19, 42.79, 41.49, <40.00 — total: 11170 kWh	– 3% reduction – reduced radiation near the facade surface
Axo view grid results				Other input parameters – Athens Weather Data, including urban conditions – South orientation – Analysis period: Extremely Hot Week (03–09/08) – Direct normal radiation – Diffuse horizontal radiation – Horizontal infrared radiation – Reflected radiation from surrounding surfaces

Figure 17. Cumulative radiation values on street level in an Athens urban canyon (cumulative radiation: direct, diffuse, and reflected radiation from all the surrounding surfaces).

The results in Figure 18, which were targeted more on the reflected part of the total radiation, showed that the percentage of the cumulative radiation that is responsible for the reflected radiation from the façade and the surrounding surfaces was reduced by around 40% with the proposed design, with again a reduced radiation close to the façade surface. However, that portion still accounted for only 6% of the total radiation, which is a relatively small amount and, therefore, would lead to the conclusion that even though the direct impact could be minimized with the proposed façade geometry to reduce the overheating of the urban microclimate, the overall impact in this regard is not significantly large.

The results from the comparative sun ray trace analyses can be seen in Figure 19. In accordance with the radiation analysis grid results, the ray trace analyses showed that a typical façade reflected the sun rays downwards towards the street level, if no other obstacles were obstructing the rays' direction. On the contrary, the proposed design reflected most of the sun rays upwards back to the atmosphere. In addition to this, the small number of rays which did not fall in that category and deviated by bouncing more horizontally due to the reflection on the different angles of the geometry surfaces, still did not bounce towards the street level, but to a much higher level above the ground. They were also scattered throughout the opposite building's length and height thanks to the convex outer geometries, avoiding undesired and increased solar focus points, as well as concentrated heat areas in the surrounding urban environment.
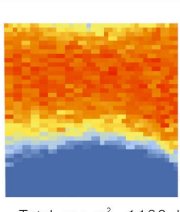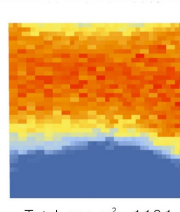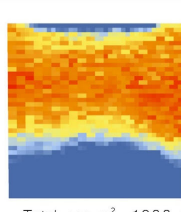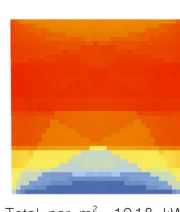
Figure 18. Analysis and partial values of the total cumulative radiation on street level in an Athens urban canyon (cumulative radiation: direct, diffuse, and reflected radiation from all the surrounding surfaces).
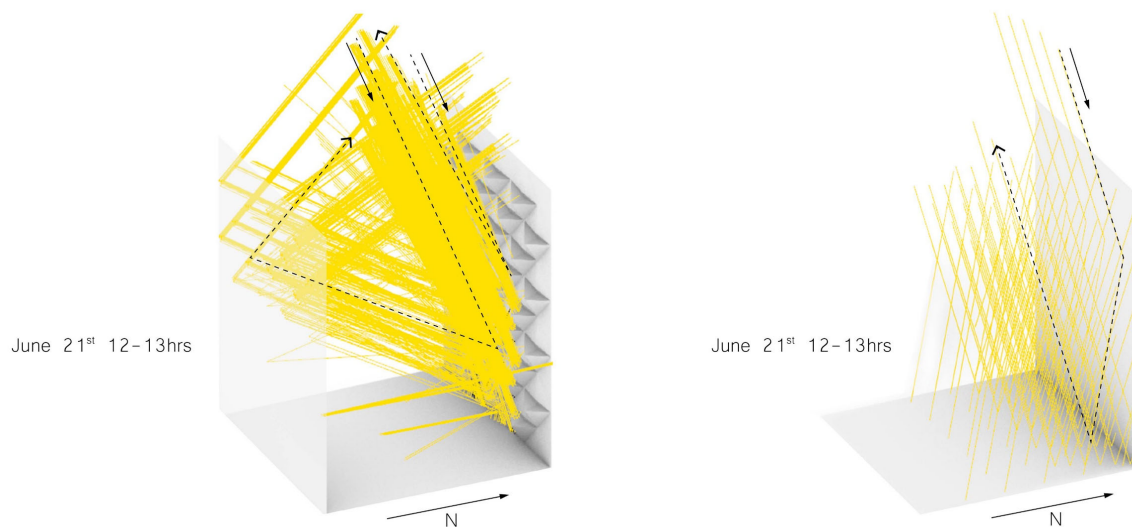

Figure 19. Comparative sun ray trace analyses of the proposed façade (left) and a typical façade in an urban street canyon, including the reflection towards the opposite building.

3.2. UHI Indirect Impact Evaluation

3.2.1. Cooling Demands Estimation Studies—Energy Use Intensity (EUI) Indicator

The cases examined are summarized in Figure 20 and relate to a great extent to the ventilation strategy and the material properties. More specifically, Case#1 assumed a small inlet and outlet opening, whereas the rest of the parameters remained unaltered with the default property of an ETFE textile with no additional treatment or coating. For comparison on the air inflow impact, Case#2 considered a larger operable effective area, to evaluate whether the air inflow resulted in a reduction of the cooling loads or led to overheating of the cavity, while in Case#3, the cavity was assigned as only slightly ventilated with minimized vents open (in reality, a fully sealed cavity cannot be achieved with the current design).

Case	Test variables			
#	Operable effective area (w / w/o air exchange between the cavity and the interior)	Night-time ventilation	SHGC value (translucent part)	Cavity width
1	0.4m² (w air exchange)	–	0.93	400mm
2	1m² (w air exchange)	–	0.93	400mm
3	0 (slightly ventilated) (w air exchange)	–	0.93	400mm
4	0 (slightly ventilated) (w air exchange)	–	0.6 (solar control coating)	400mm
5	0 (slightly ventilated) (w air exchange)	–	0.6 (solar control coating)	150mm
6	0.4m² (w scheduled air exchange)	yes	0.6 (solar control coating)	400mm
7	0.4m² (no natural ventilation) (w/o direct air exchange)	–	0.6 (solar control coating)	400mm
8	w/o air exchange, no double skin function or natural ventilation (no cavity thermal zone), exterior facade skin only as sun-shading			

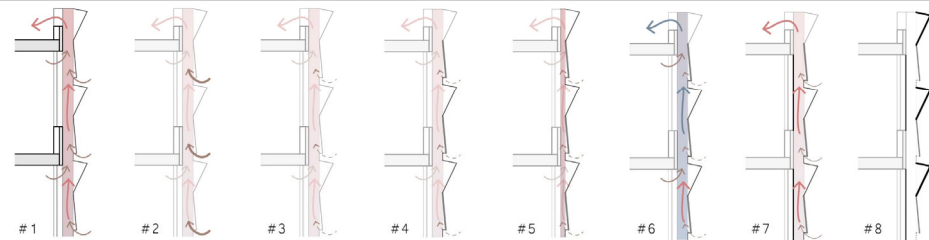#1   #2   #3   #4   #5   #6   #7   #8

Figure 20. Overview of the case studies and test parameters for the EUI calculation studies for the cooling loads.

From Case#4 on, the SHGC of the translucent textile had a lowered value, and in Case#5, a smaller cavity size was tested. Case#6 explored the ventilation scenario for an only night-time ventilation to aid the exhaust of the accumulated heat that is trapped inside the cavity during the day, with a scheduled air exchange between the thermal zones. In Case#7, no natural ventilation was enabled through the cavity, with no direct air exchange between the thermal zones, but allowing only heat exchange through the construction and some air flow through the cavity to the top exhaust. Lastly, the Case#8 scenario explored the possibility to avoid the double skin function during the summer, eliminating the cavity effect and not allowing any natural ventilation or air exchange to the interior. In this case, the façade skin works only as an independent exterior shading device, without creating any in-between thermal zone.

As for the existing single façade case study, to avoid complications with natural ventilation strategies, which was an unknown variable in this case, and to make comparison as objective as possible, the air loads system was assumed to be conditioned and mostly functioning through mechanical ventilation, while the glazing type was assigned as a generic double-pane window without low-e coatings. Additionally, in the cases where natural ventilation was enabled, it was set to be activated with a delta temperature setpoint at −2 °C in relation to the cooling setpoint.
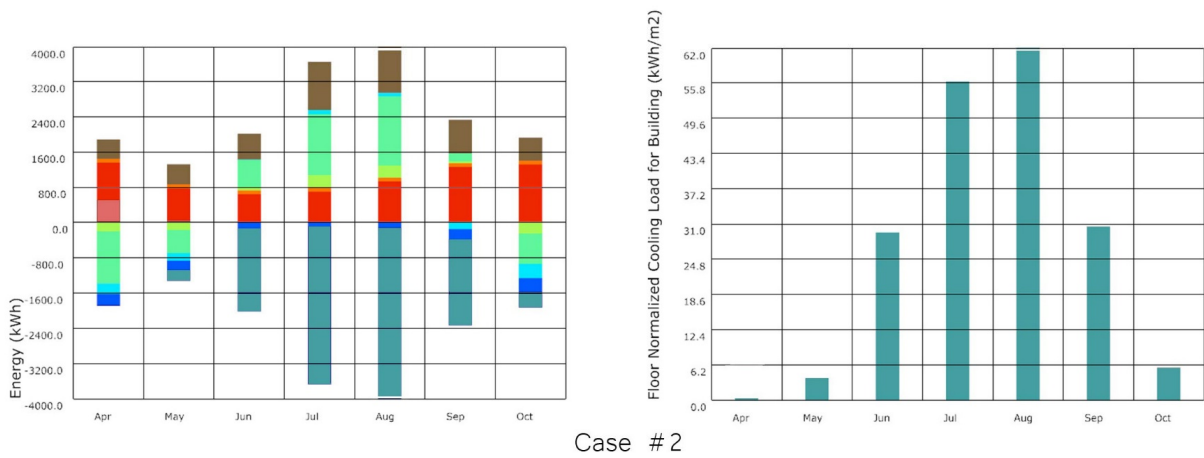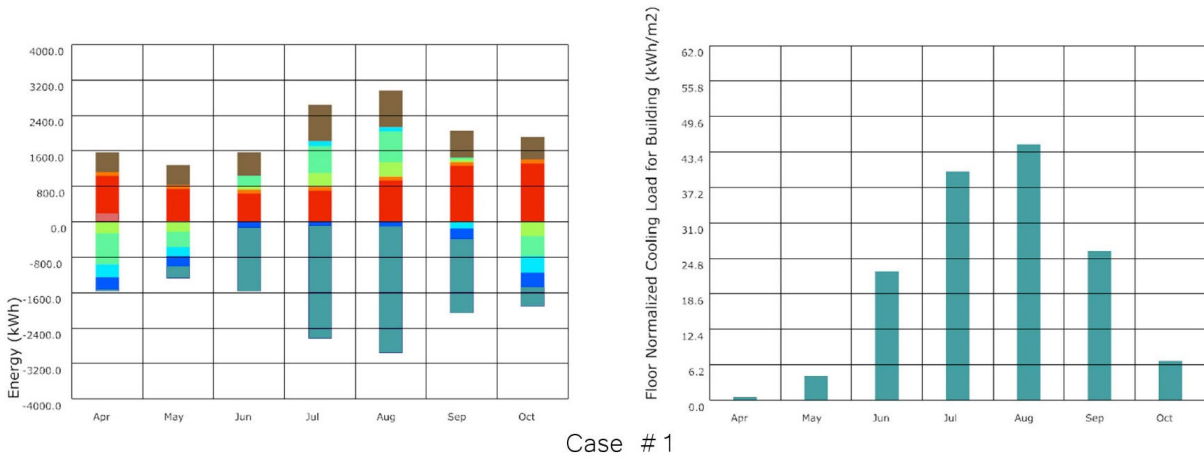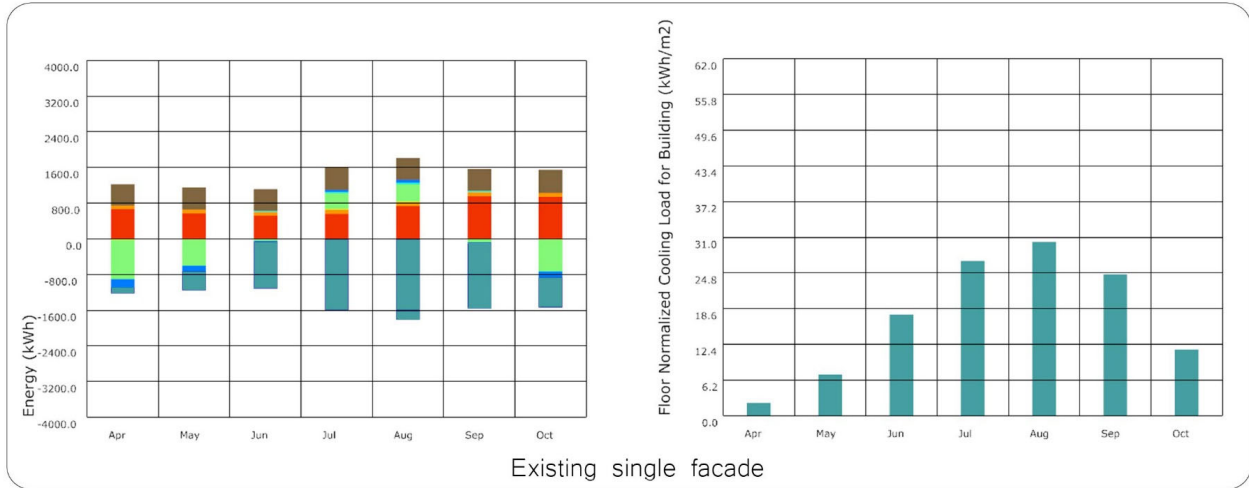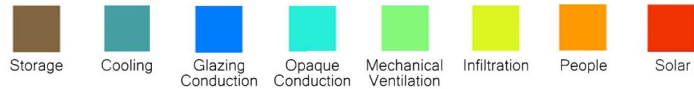
A summary of the results for the cooling loads per area can be found in Figure 21, whereas the difference in percentage compared to the existing single façade was also calculated. The energy balance (in kWh) and the floor-normalized cooling load for the building (in kWh/m²) charts for the analyzed period are shown below for each corresponding case (Figure 22).

Case	Cooling loads per m² (Energy Use Intensity)	Difference in %
Existing single facade	**120 kWh/m²**	
#1	145.1 kWh/m²	+21%
#2	188.7 kWh/m²	+57%
#3	113.5 kWh/m²	−5.4%
#4	104.4 kWh/m²	−13%
#5	109.7 kWh/m²	−8.5%
#6	102.3 kWh/m²	−15%
#7	104.4 kWh/m²	−13%
#8	95 kWh/m²	−21%

Figure 21. Results of the EUI calculations for the cooling loads of the case studies shown in Figure 20.

From the above studies, it can be concluded that during the cooling-dominated periods, the air inflow inside the cavity led to an overheating of the building due to the greenhouse effect inside of it. A higher amount of air inflow resulted, therefore, in an increase in the cavity temperature, as can be seen in Cases#1 and #2 with an increase of 21% and 57% of the cooling demands, respectively. The increase was also caused by the absence of additional solar control coatings on the textile surface, which is one of the variables that influenced the cooling demands value, as can be seen in Case#4, with a reduction of −13%, as a result of the reduction of the SHGC coefficient value. A larger cavity also had a better impact than a smaller one in that respect, because the smaller one would also lead to a faster increase in the air flow temperature inside the cavity. When it comes to the ventilation strategies, what can be estimated is that it would be more efficient to achieve a combination of night-time ventilation to exhaust the accumulated hot air during the nonoperating times of the office building, when it is not occupied, and to minimize the air exchange between the different thermal zones during the day, to avoid discomfort and to minimize the need for air conditioning. More specifically, by comparing Cases #6, #7, and #8, it can be concluded that the least interaction and air exchange between the interior and the exterior environment has the most beneficial impact for the reduction of the cooling loads, whereas the façade system would work better merely as an exterior shading device, reducing the solar heat gains to the building's interior by 21%, without interfering as a double façade and as a result trapping warm air in the in-between space. There is, therefore, no other added benefit during the summer, apart from the shading effect.

In this respect, a supplementary evaluation study involved the comparison of the shading effect of the proposed façade skin to other typical shading devices and their impact on the reduction of the cooling demands, taking, as comparison, the unshaded existing façade case and Case#8 from the previous study (here named as Case#1). The examples to be compared with were, namely, typical exterior horizontal venetian blinds and an exterior fabric roller shade or perforated metal screen. In both of these cases, it was assumed that the shading is on, if the outside temperature exceeds the cooling setpoint of 24 °C and if the horizontal solar radiation exceeds the setpoint of 400 W/m².
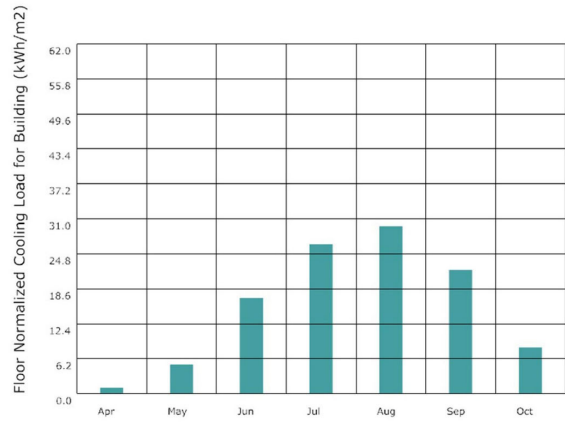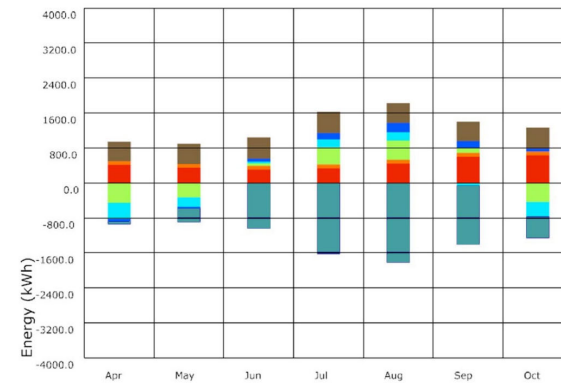
Existing single facade

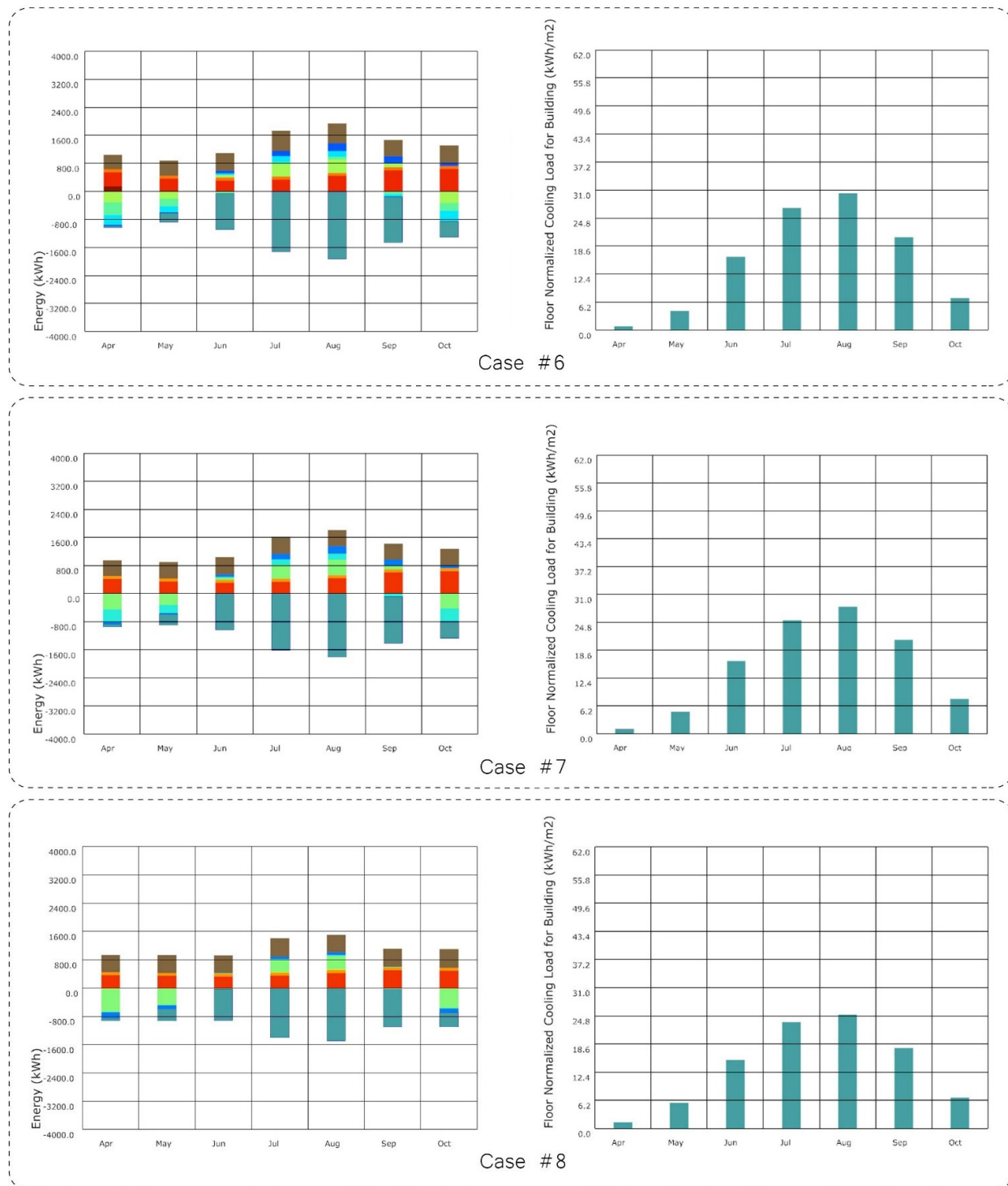Case #1

Case #2
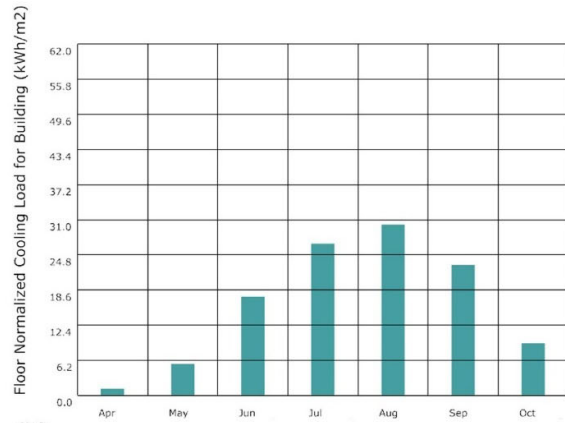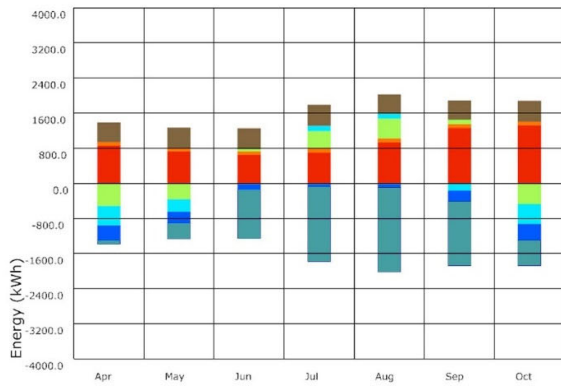
Case #3
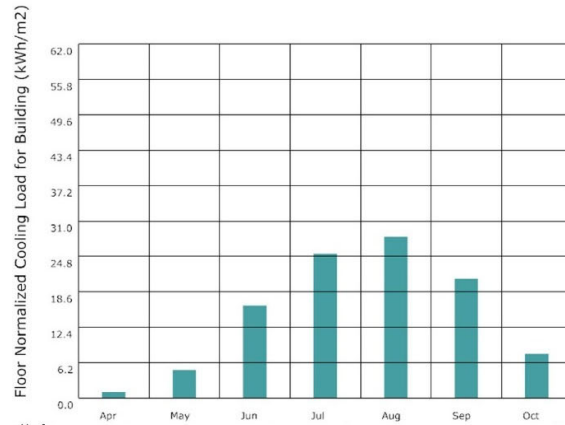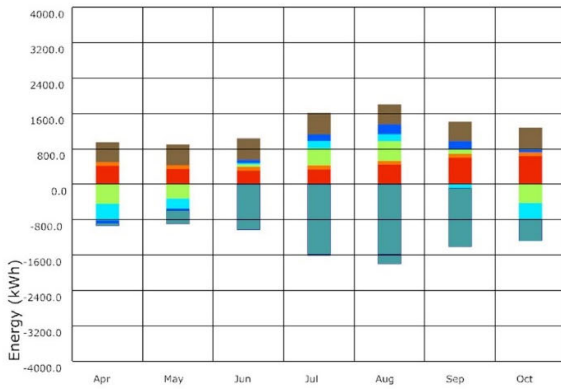
Case #4

Case #5

Figure 22. Energy balance charts (**left**) and EUI of the cooling loads charts (**right**) for each case study shown in Figure 20.

The results summarized in Figures 23 and 24 showed no significant difference between the three shading examples, even with a marginally better performance of the typical shading devices. The effect of the façade skin could not outperform the rest during

this comparison to make it competitive against more cost-efficient and simpler shading solutions, but at the same time it still showed a similar performance. The façade performance during the summer is, therefore, not sufficient on its own to justify such a design. However, this led to the next evaluation round, to assess whether the dynamic movement would bring additional benefits through its seasonal function and adaptation by creating the multiple-cavity double skin function during the winter.

Case	Shading type scenario	Cooling loads per m² (Energy Use Intensity)	Difference in %
#	Existing single facade with no sun-shading	**120 kWh/m²**	
1	Proposed facade skin design only as sun-shading	95 kWh/m²	−21%
2	Typical exterior horizontal venetian blinds*	92 kWh/m²	−23%
3	Exterior fabric roller shade/perforated metal screen*	89.5 kWh/m²	−25%

*Shading is on, if the outside air temperature exceeds the Cooling Setpoint of 24°C
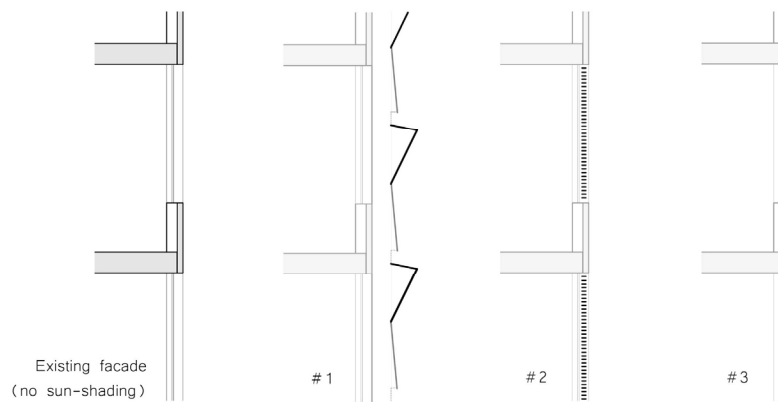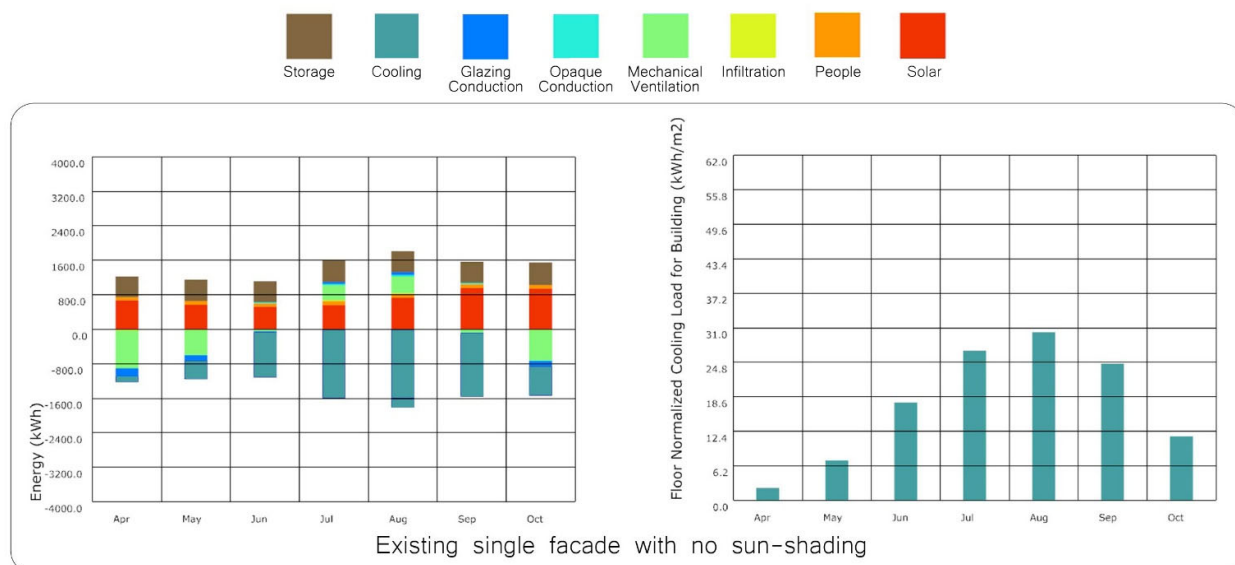and if the horizontal solar radiation exceeds the SetPoint of 400 W/m²

Figure 23. Overview of the cooling loads results for the shading type scenarios and comparison to the existing single façade with no external sun-shading and the corresponding cases in schematic graphs.
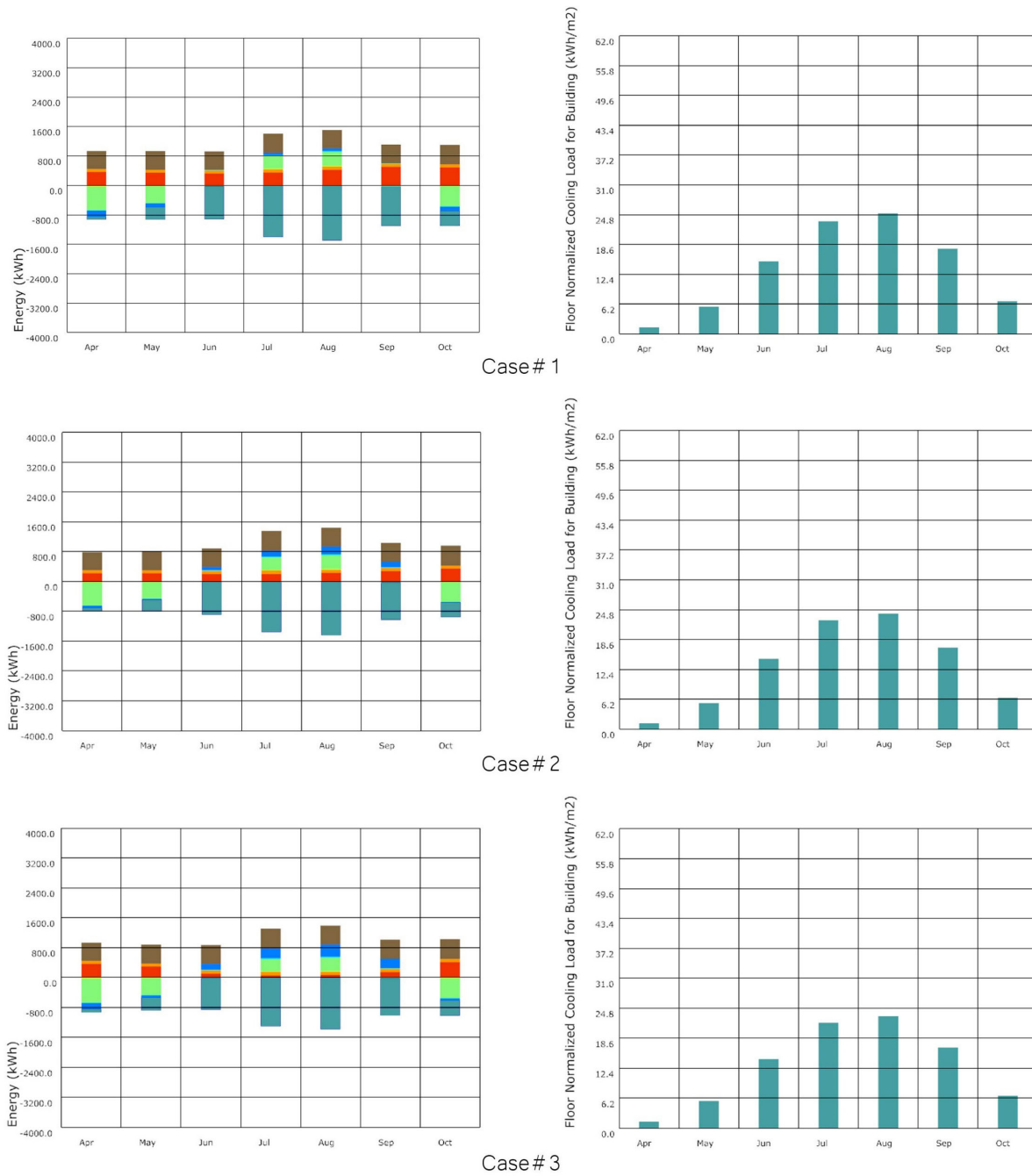
Figure 24. Energy balance charts (**left**) and EUI of the cooling loads charts (**right**) for each case study shown in Figure 23.

3.2.2. Thermal Analysis—Heat and Air Flows Simulations

The results from the winter situation (Figure 25) showed that there is an increase in the surface temperature around the inner boundary of up to 25 °C with a further increase on the top surfaces of the cavity boundaries due to the air and heat stratification. Similar results were found through the THERM static temperature fluctuation simulation, which showed a heat buffer accumulated outside the insulation layer, reducing the heat losses

and the temperature difference between the interior and the exterior during the cold months. It can also be noticed that the simulations realized through SimScale capture only an hour of operation and, in that way, show the effect in its starting moments when the cavity begins to heat up, while the THERM model shows the temperature fluctuations as a static building construction with no incoming airflow, which, however, receives a constant additional radiation heat on the outer boundary layer. In this sense, Case#1 and the THERM model can be approximate representatives of the two boundary conditions, the beginning and the peak of the thermal effect, respectively, with the SimScale one to also highlight the reverse situation when the model slowly transcends back to its original cool state after the solar radiation intake is reduced during the late afternoon hours.
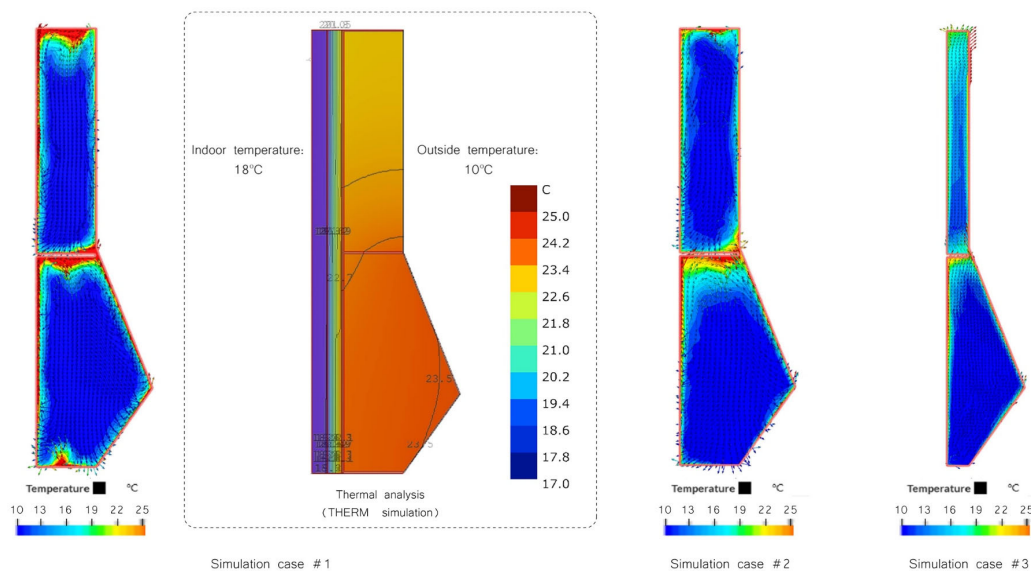

Figure 25. Convective heat transfer analysis simulation results for the winter situation.

In addition, in Case#2, there is an increase in the temperature inside the cavity and the convective effect of the inner pyramid volume is also more evident, which can be justified by the increase in the heat flows induced by the increased air movement that is heated up when entering the cavity. However, this creates, at the same time, a constant air influx, which leads to heat losses at similarly high speeds, so the heat buffer effect is then being reduced. Lastly, in Case#3, the narrower cavity on top also led to an increase in temperature due to less air volume requiring less time to reach a higher temperature. However, as seen by the cooling demands analysis and despite possible winter benefits, a narrow cavity would cause an overheating during the summer, which is more critical to mitigate for the scope of the current study. It can, therefore, be concluded that the function during the cold seasons as a multiple-cavity system can have the potential to offer additional benefits as a thermal buffer zone for the reduction of the heat losses.

Regarding the summer scenario, the results summarized below (Figure 26) showed similar behavior inside the cavity, with higher temperatures on the boundary surfaces and in the narrow air volumes. The difference here is that there is a slight reduction of accumulated heat when there are no air inlets between the interior building spaces and the continuous cavity zone, as in Case#2. In accordance with the conclusions from the cooling demands analysis, the air entering the cavity is warmer than the interior, causing overheating of the cavity and introducing hot air to the interior instead, in a greenhouse manner. The temperatures reached are above the outdoor ambient temperature, ranging in average from 35 °C–37 °C, with some local intensified boundary areas that exceed those limits. This can also be seen in the areas around the air inlets, where there is a local increase

in temperature. Case#3 showed negligible difference compared to Case#2 and also needed to be slightly modified to avoid continuity errors caused by excluding air inlets, so a minimum area of air inlets was also assigned at the bottom of the outer layer instead, to comply with the pressure outlet on top.
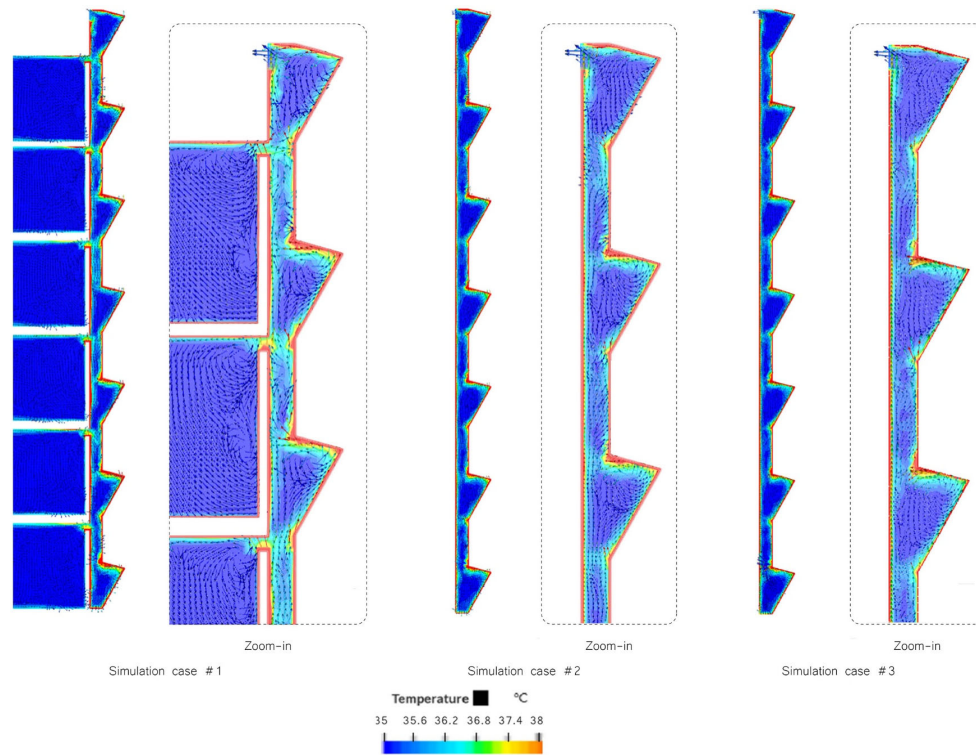

Figure 26. Convective heat transfer analysis simulation results for the summer situation.

4. Discussion

As a summary from the above evaluation studies, regarding the direct impact of the façade design on the UHI effect, it can be concluded that the proposed geometry showed a reduction on the reflected solar radiation at the street level and on the urban heat intensification at a microclimate level. This was more apparent, especially, close to the façade surface and through dissipating the incoming solar rays from being reflected and accumulated inside the urban canyons. The part of the reflected solar radiation on the urban surroundings that the building is responsible for was, therefore, significantly reduced. However, the direct impact on the overall building's share on the UHI effect still remained relatively small compared to the cumulative solar radiation that is caused by other sources and is not obstructed by other mitigation strategies (Figure 27). In this sense, it can be assumed that a reduction on the building's direct contribution is not as impactful as the indirect one, which concerns the building's energy performance.

The indirect analysis studies and comparative evaluations provided some insights on the environmental and energy performance of the proposed design. It was concluded that during the cooling-dominated periods, the façade skin has a higher performance when functioning only as an exterior shading device, without interfering with the building's air inflow, but working as a separate exterior structure obstructing the incoming solar radiation. By doing so, the solar heat gains could be reduced and, consequently, so could the building's cooling demands by about 21%.
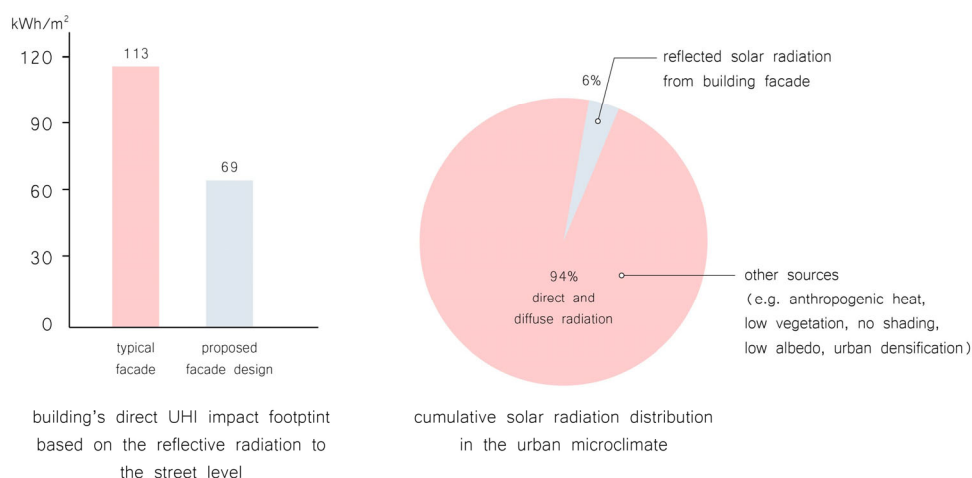
Figure 27. Charts summarizing the direct impact evaluation conclusions.

Nevertheless, the shading impact of the proposed design did not outperform other commonly used typical exterior shading systems, but still performed almost equally well. The difference in the current design was due to the dynamic performance of the façade's passive mechanism that shifted to the multiple-cavity double façade during the winter and led to additional benefits in the reduction of the heat losses through the building construction. However, solely in relation to the UHI effect, this was a secondary function that was not directly related to the phenomenon and mitigation method, since the reduction of the cooling loads has the main and more impactful role. It could be, therefore, said that the overall energy performance of the building can, on one hand, be improved by integrating such a passive adaptive façade system, when being evaluated through an annual operation basis. On the other hand, the environmental performance, merely in relation to the reduction of the building's indirect UHI impact, was not much different to that by simply implementing standard exterior shading systems or by adopting other standard solutions (Figure 28).
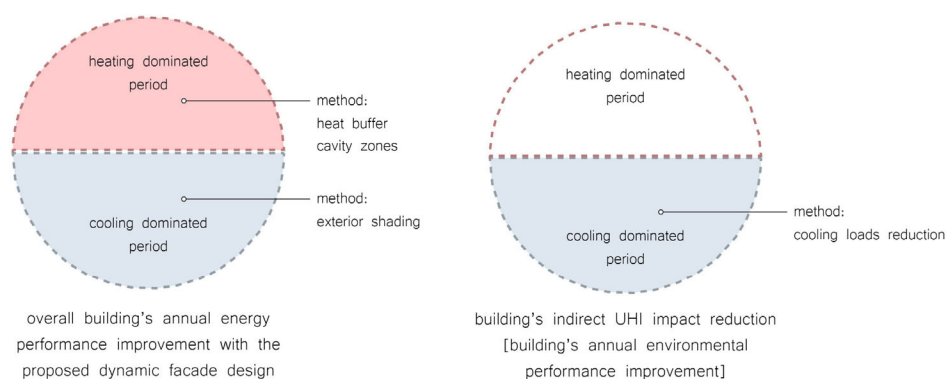

Figure 28. Charts summarizing the indirect impact evaluation conclusions.

As a conclusion from the research process and assessment methodology, it could be argued that the evaluation of the proposed façade system in the end depended, to an extent, on the comparison benchmarks and the perspective of evaluation. As seen during the initial stages of the research layout, since UHI concerns a multilayered environmental issue, the evaluation also lay on multiple levels. Some of these observations can be summarized below and are illustrated in the diagrams in Figure 29:

- If the system is evaluated as a standalone solution and only compared to the existing building situation before the retrofit, then the impact on the UHI effect is significant, more visible on the indirect one, but also contributing positively to the direct one.
- If the comparison lies only on the direct impact, it has a better effect compared to both the existing façade and other shading devices, since the judgement lies on the materiality and reflectivity degree of the building's geometry. In this case, however, it is also noted that the building's direct impact is not high enough, compared to other potentially more commonly applied mitigation strategies and interventions, such as vegetation or urban shading, to be able to provide a noticeable improvement on the UHI reduction in the urban microclimate.
- If only the indirect effect is evaluated, then it has an impact on the reduction of the building's cooling demands of the existing building situation, working as an external sun-shading skin and reducing the solar heat gains during summer. However, when compared to other shading devices on the same criterion, then the effect is similar, if not slightly less.
- If the evaluation lies only on the impact on the UHI effect as an isolated scenario, as it was the main objective of the study, then the façade design performed overall better than the other shading devices, because of the additional contribution in the direct impact on the urban microclimate.
- When the design is additionally being assessed as an overall dynamic façade system, including both energy and environmental performance, it brings added benefits to the building's annual operation. This is achieved by functioning as a closed-cavity double façade during the winter and, thus, reducing heat losses. In addition to that, even though the cooling demands are reduced almost equally compared to the other shading devices, the last ones operate only during warm and sunny periods.
- When compared to similar state-of-the-art façade systems, the question lies mostly on feasibility variables, such as cost-effectiveness, operation complexity, and maintenance. However, merely on the energy aspect, for example, a typical double skin façade would only have positive effects during the winter, especially in a warm climate such as the Mediterranean one, and would possibly require additional sun-shading within the cavity, since it would cause overheating during the summer. On the other hand, the proposed façade design has an annual dynamic operation, shifting from sun-shading function during the cooling-dominated periods to double façade during the heating-dominated ones.

The assessment is, therefore, in general greatly dependent on the reference points and what the objective focus in each situation is.

Finally, to spark further discussion, a comparison of the reflective values of the current design's shading membranes with other applied UHI mitigation strategies aimed to evaluate the impact of the materiality of the proposed design to other common practices and to reflect on the possible benefits of each case. The examples chosen for this comparison were a standard white paint, an ultra-white one, cool-colored paints, and retro-reflective materials, because they are based on the principle of radiative cooling, which is a passive cooling technology that offers potential to reduce space cooling cost and tackle the UHI effect.

From the above applications, retro-reflective materials can have a more targeted contribution to the UHI effect by avoiding the reflection towards the urban environment and, therefore, are a more competitive solution against the design of the current project. The question that followed then was to which extent of building applications and context this solution would be equally beneficial without increasing the complexity of the intervention.

Figure 29. Building's energy and environmental performance comparative evaluation charts.

It can be assumed, for example, that in a fully opaque façade, the application of retro-reflective materials could be a more efficient solution, since it is simpler to apply, more time- and cost-efficient, and can achieve the same or even better results, since a PTFE membrane can achieve about 70% of solar reflection, whereas it can be easily replicated in many similar situations. In contrast, once the window-to-wall ratio starts increasing, then more parameters are intertwined, with the user's inner comfort having a more central role. In this case, retro-reflective materials alone will not be sufficient to lower the building's cooling demands and additional measures will be required, such as solar and ventilation control. In this sense, the proposed design can probably gain advantage, because of the

added benefits it provides through an integrated solution with more variables taken into account and incorporated into its dynamic and seasonal function.

Under the studied application scenario, the question and boundary conditions lie mostly on the level of complexity up to which simpler solutions are no longer self-sufficient as a standalone solution to provide high enough energy and environmental performance, and consequently to have a significant impact on the UHI effect and urban microclimate. This threshold is where, due to the complexity of the context, the choice for the current design can be justified, however seen as one building application and not a repeated strategy. Once the complexity and requirements increase even more, on the other hand, then a passive mechanism is also potentially not enough as an argument by itself and should be combined or overridden by a more reliable mechanical control and programmed automation. In the end, each case is better suited for a certain application range, but the design goal and decisions remain, nevertheless, intact, aiming to provide a solution which is able to develop a façade system with both high overall performance and little internal complexity.

In addition, throughout the research process, the analysis studies were realized in different façade test scales, ranging from component to façade segment to the urban level, as well as the building's interior, whereas it was observed that the simulation studies could also be grouped based on the objective and focus of interest. This clustering could offer an interesting potential and a recommendation for future development, to create a digital tool as a result of this methodology toolchain (Figure 30). To this regard, the design process relied highly on the parallel development and aid of computational tools for the energy and environmental simulation and performance evaluation of the design. This workflow promotes the importance of the digital tools in the service of the architect, designer, or building physicist, among other relevant disciplines. In this direction, the current project followed a systematic step-by-step workflow and explored the potentials of this method with the objective to evaluate the design and building's performance. The design itself can, therefore, be perceived as just a demonstration case study and outcome of the above iterative computational workflow that is applied in practice, out of many other possible alternatives. In this sense, a different scenario with a different initial geometry input and another set of parameters and requirements would lead to a different design result. At the same time, the study objectives and the workflow remain intact as the core of the feedback-optimization process and as the available toolset at disposal to aid the performance assessment and design development, as shown in Figure 31.

However, a common challenge that was also encountered during the current process concerned compatibility issues due to the different versions of the various Grasshopper plug-ins, components, and simulation engines, which can occasionally lead to simulation errors or discrepancies in the calculations, resulting in a time- and energy-consuming troubleshooting process. In the current research, since it was based mostly on comparative study analyses, certain assumptions in the boundary conditions used and small discrepancies in the result accuracies were taken into account and did not have a significant impact on the conclusions drawn. For future development, resolving these issues and creating a more straightforward, compact, and user-friendly interface for professionals without necessarily a computational background would be recommended as a follow-up of the presented logic. This would provide an efficient and less-fragmented workflow, without the division into many separate scripts, which might additionally require significant computational processing time or lead to information losses during the modeling transition. The focus would then be placed mostly on the energy- and environmental-driven design optimization by inserting the set of façade geometry parameters and postprocessing the output results in a more efficient feedback-loop design process, without the need to directly interfere with the background computational setup. What distinguishes the presented iterative process is that at its core it is not bound to the specific design each time, but rather offers a workflow platform as an independent step-by-step guideline, with the design's performance assessment as a clear objective.
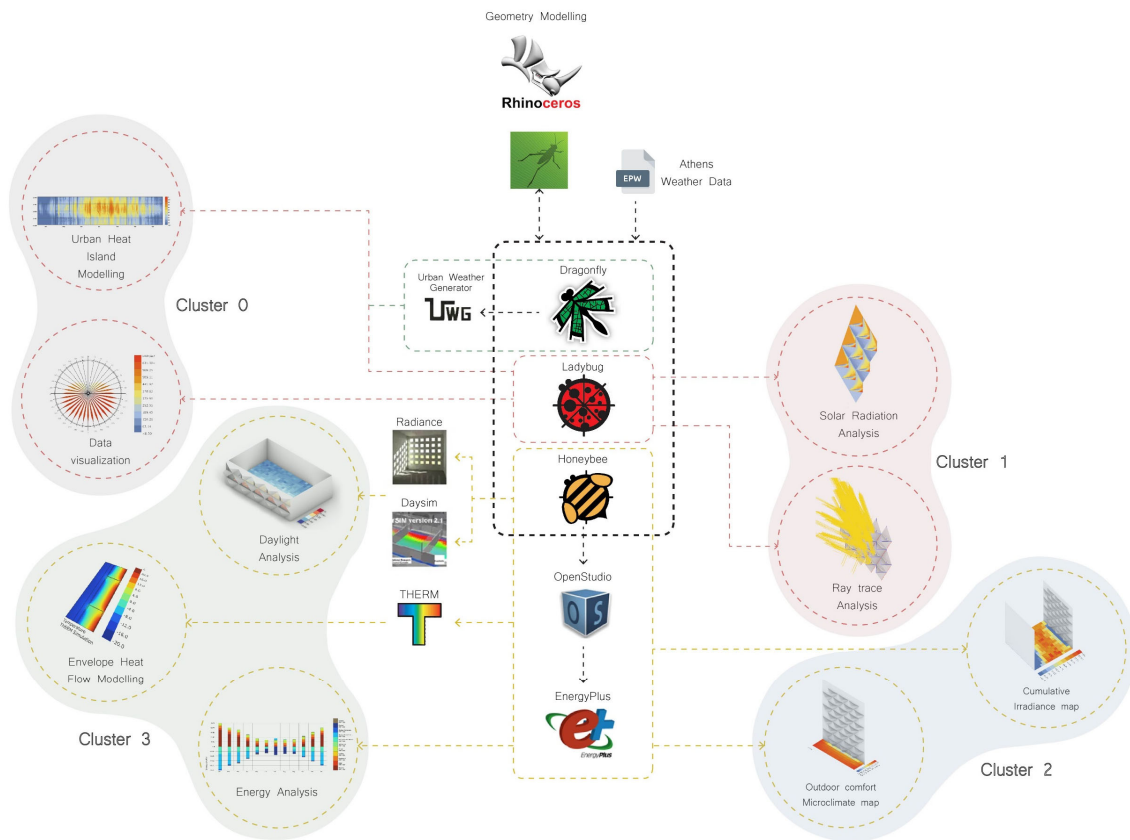
Figure 30. Subdivision of the followed computational workflow and clustering overview for the development of the digital tool.
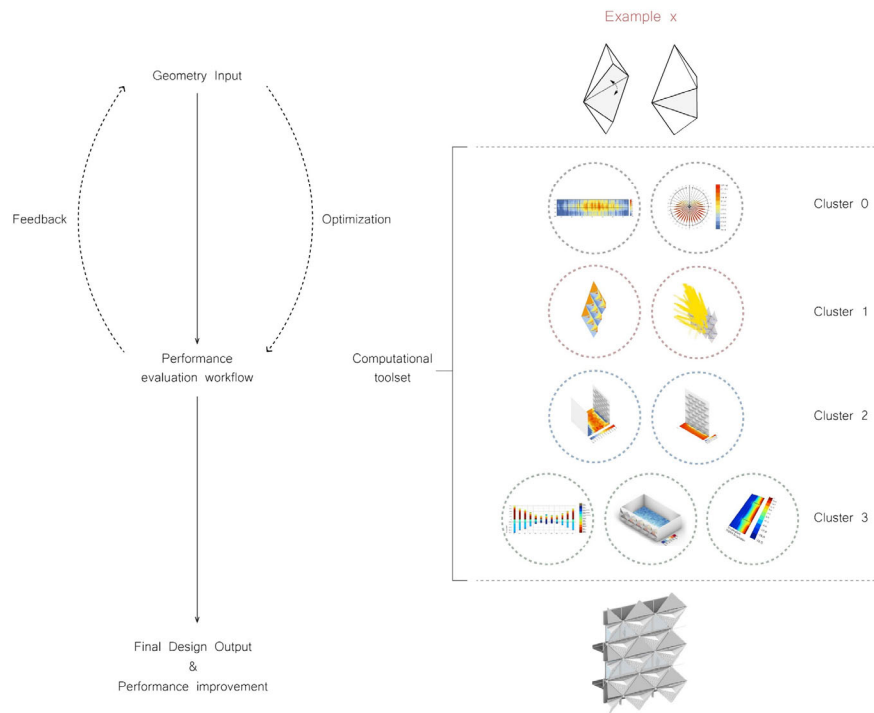

Figure 31. The feedback-optimization logic of the performance evaluation as part of the computational tool workflow and the current design as an example of its application in practice.

Lastly, it seems important to address the need for experimental measurements to validate the results discussed in this paper and demonstrate the potential of the proposed workflow. While this was out of the scope of the present study, experimental validation with real scale prototypes is regarded as the clear next step to verify the results and continue developing the proposed technical solutions.

5. Conclusions

The proposed design was based on the development of a façade shading system, which featured a double function during the summer and winter. This was enabled through a dynamic movement triggered by the passive autoreactive behavior of the SMAs and controlled through a pivot mechanism. The research question was focused on the evaluation of the above dynamic operation and the adaptive movement of the system in terms of the influence on the building's direct and indirect UHI impact. To address this objective, the performance goals aimed, on one hand, to increase the reflective effect towards the atmosphere through optimizations in the geometry and movement, and, on the other hand, to reduce the building's cooling demands by reducing the incoming solar heat gains and by means of self-shading.

In the end, the conclusions from each evaluation study led to the observation that the presented façade design with an optimized faceted geometry and diagonal arrangement could potentially reduce the building's direct impact on the urban microclimate with a reduction of about 40% of the reflected portion of the total solar radiation and a more apparent effect close to the façade surface. However, compared to other possible mitigation strategies, the impact was negligible in making a difference in the overall UHI reduction, with only 6% of the total cumulative radiation on the street level resulting from the reflected radiation from the façade surface. On the contrary, the reduction of the cooling demands and, consequently, the indirect UHI impact was more noticeable, with the proposed façade design able to reduce the cooling loads by about 21%.

From the above studies, it can be summarized that there is potential to explore and enhance the use of SMAs in façade applications to increase the building's performance, thanks to their ability to enable dynamic movements with little energy and material required. The challenges lie mostly in the feasibility, the user's control, and operation cycles of such autoreactive systems and their implications when placed in a broader context. To this regard, it is important to critically evaluate to what extent their implementation can lead to added benefits, taking more parameters into account in practice during the entire life-cycle operation. The question, and challenge, therefore, is how to optimally integrate passive strategies to promote sustainability through adaptiveness and smart material-based solutions and under which conditions, to be able to adequately adapt the indoors to the outdoor environmental changes and maximize both the energy and environmental performance.

Last, but not least, an important contribution of the current project is the integrated systematic design approach through a computational workflow rather than the final design result, and it can be relevant to explore further its potentials for possible applications. This is because it can offer a universal computational methodology and a series of systematic and comprehensive stages for the façade study and evaluation that can be developed and incorporated as a useful digital tool for the service of a broad range of professionals in the field.

References

1. Santamouris, M. Heat Island Research in Europe: The State of the Art. *Adv. Build. Energy Res.* **2007**, *1*, 123–150. https://doi.org/10.1080 /17512549.2007.9687272.
2. Salvati, A.; Roura, H.C.; Cecere, C. Assessing the urban heat island and its energy impact on residential buildings in Mediterranean climate: Barcelona case study. *Energy Build.* **2017**, *146*, 38–54. https://doi.org/10.1016/j.enbuild.2017.04.025.
3. Golden, J.S. The Built Environment Induced Urban Heat Island Effect in Rapidly Urbanizing Arid Regions—A Sustainable Urban Engineering Complexity. *Environ. Sci.* **2004**, *1*, 321–349. https://doi.org/10.1080/15693430412331291698.
4. Giannopoulou, K.; Santamouris, M.; Livada, I.; Georgakis, C.; Caouris, Y. The impact of canyon geometry on intra Urban and Urban: Suburban night temperature differences under warm weather conditions. *Pure Appl. Geophys.* **2010**, *167*, 1433–1449;. https://doi.org/10.1007/s00024-010-0099-8.
5. Papamanolis, N.; Dimelli, D.; Ragia, L. The urban heat island intensities in Greek cities as a function of the characteristics of the built environment. Presented at 9th International Conference on Urban Climate jointly with 12th Symposium on the Urban Environment, Toulouse, France, 20–24 July 2015.
6. Founda, D.; Santamouris, M. Synergies between Urban Heat Island and Heat Waves in Athens (Greece), during an extremely hot summer. *Sci. Rep.* **2017**, *7*, 10973. https://doi.org/10.1038/s41598-017-11407-6.
7. Santamouris, M.; Papanikolaou, N.; Livada, I.; Koronakis, I.; Georgakis, C.; Argiriou, A.; Assimakopoulos, D.N. On the impact of urban climate on the energy consumption of buildings. *Sol. Energy* **2001**, *70*, 201–216.
8. Phelan, P.E.; Kaloush, K.; Miner, M.; Golden, J.; Phelan, B.; Silva, H.; Taylor, R.A. Urban Heat Island: Mechanisms, Implications, and Possible Remedies. *Annu. Rev. Environ. Resour.* **2015**, *40*, 285–307. https://doi.org/10.1146/annurevenviron-102014-021155.
9. Wei, Z.G.; Sandstroröm, R.; Miyazaki, S. Shape memory materials and hybrid composites for smart systems: Part I Shape-memory materials. *J. Mater. Sci.* **1998**, *33*, 3743–3762. https://doi.org/10.1023/A:1004692329247.
10. Addington, M. *Smart Materials and Technologies in Architecture*; Routledge: London, UK, 2012; https://doi.org/10.4324/9780080480954.
11. EnergyPlus. Available online: https://www.energyplus.net/ (accessed on 25 April 2021).
12. Nakano, A. Urban Microclimate: Uwg: Download. Available online: https://urbanmicroclimate.scripts.mit.edu/uwg.php/ (accessed on 15 December 2021).
13. OpenStudio. Available online: https://openstudio.net/ (accessed on 15 December 2021).
14. Radiance–Radsite. Available online: https://radiance-online.org/ (accessed on 15 December 2021).
15. Reinhart, C.; DAYSIM. Software Informer. Available online: https://daysim.software.informer.com/ (accessed on 18 April 2021).
16. THERM Software Downloads. Windows and Daylighting. Available online: https://windows.lbl.gov/tools/therm/ (accessed on 18 April 2021).
17. Simulation Software: Engineering in the Cloud. Available online: https://www.simscale.com/ (accessed on 3 May 2021).
18. Zhou, J.; Chen, Y. A review on applying ventilated double-skin façade to buildings in hot-summer and cold-winter zone in China. *Renew. Sustain. Energy* **2010**, *14*, 1321–1328.
19. Matzarakis, A.; Balafoutis, C. Heating degree-days over Greece as an index of energy consumption. *Int. J. Climatol.* **2004**, *24*, 1817–1828. https://doi.org/10.1002/joc.1107.
20. Carlucci, S.; Causone, F.; Biandrate, S.; Ferrando, M.; Moazami, A.; Erba, S. On the impact of stochastic modeling of occupant behavior on the energy use of office buildings. *Energy Build.* **2021**, *246*, 111049. https://doi.org/10.1016/j.enbuild.2021.111049.
21. Cartalis, C.; Synodinou, A.; Proedrou, M.; Tsangrassoulis, A.; Santamouris, M. Modifications in energy demand in urban areas as a result of climate change: An assessment for the southeast Mediterranean region. *Energy Convers. Manag.* **2001**, *42*, 1647–1656.
22. Leonidaki, K.; Kyriaki, E.; Konstantinidou, C.; Giama, E.; Papadopoulos, A.M. Thermal performance of office building envelopes: The role of window-to-wall ratio and thermal mass in Mediterranean and Oceanic climates. *J. Power Technol.* **2014**, *94*, 1–7.
23. Fuliotto, R.; Cambuli, F.; Mandas, N.; Bacchin, N.; Manara, G.; Chen, Q. Experimental and numerical analysis of heat transfer and airflow on an interactive building façade. *Energy Build.* **2010**, *42*, 23–28.
24. He, G.; Shu, L.; Zhang, S. Double skin façades in the hot summer and cold winter zone in China: Cavity open or closed? *Build. Simul.* **2011**, *4*, 283–291. https://doi.org/10.1007/s12273-011-0050-7.
25. Pappas, A.; Zhai, Z. Numerical investigation on thermal performance and correlations of double skin façade with buoyancy-driven airflow. *Energy Build.* **2008**, *40*, 466–475.